

Coastal Water Monitoring and Algorithm Development for Hyper-Spectrum Sensor

*Ichio ASANUMA**, *Shinya Odagawa***, *Chiaki Kobayashi***, *Masaki Kawai***, *Masatane Kato***,
*Genya Saitoh****, and *Akihiro Kishima****

*The Tokyo University of Information Sciences, 1200-2, Yato, Wakaba, Chiba, Japan 265-8501

**The Earth Remote Sensing Data Analysis Center, 3-12-1, Kachidoki, Chuo, Japan 104-0054

***The University of Tohoku, 1-1, Tsutsumi, Amamiya, Aoba, Sendai, Japan 981-8555

ABSTRACT

The airborne hyper-spectrum sensor was deployed over the coastal water to monitor bio-optical properties and to develop algorithms to estimate chlorophyll-a concentration, diffuse attenuation coefficient, and colored dissolved organic matter. The hyper-spectrum data will cover the missing information among bands, which are spectrum bands in the traditional satellite borne ocean color remote sensors. The new concept of algorithms using hyper-spectrum information will be discussed for the apparent optical property (AOP) and the inherent optical property (IOP). The test study area includes the coastal water with high turbidity and clear water within a range, and includes biologically damaged coastal floor.

Keywords: hyperspectral imaging, ocean color, CDOM, Kd, chlorophyll

1. INTRODUCTION

In the history of the ocean color remote sensing, the coastal water is the further problem for the algorithm development including atmospheric correction and/or bio-optical algorithm (Wang et al., 2007, Chami, 2007, O'Reilly et al., 1998). Especially, the colored dissolved organic matter (CDOM) and the suspended particles in the case II water are unavoidable substances to be analyzed so as to obtain the chlorophyll-a concentration from remotely sensed data (IOCCG, 2000). As the case II water, located along the coast or on the continental shelf, exhibits the non-zero upwelling radiance at the red or in the near infra-red bands, it is difficult to remove an atmospheric contribution from the upwelling radiance in the short visible bands like 400 and 500 nm. In contrast, the case I water with only phytoplankton exhibits the zero upwelling radiance in the long wavelength and the current atmospheric correction works very well to remove the atmospheric contribution in the short visible bands. The accuracy of the atmospheric correction restricts the accuracy in the bio-optical algorithm combining the bands in the short visible bands.

Although, there remains an uncertainty in the atmospheric correction in the short visible bands over the case II waters, the bio-optical algorithms were proposed to estimate chlorophyll-a concentration, the CDOM, and the

diffused attenuation coefficient at 490 nm (Kd490), where

Kd490 is used to represent the concentration of suspended particles. The chlorophyll-a concentration, CDOM and Kd490 are given by the empirical functions with the ratios among bands, but with the uncertainty in the coastal water. Sometimes, by the exceeding atmospheric correction from red and infra-red bands to the green and blue bands, the negative radiances are observed in the blue and green bands with resulting failures in estimating chlorophyll-a concentration and so on. Among ocean color scientists, there were many efforts to obtain the accurate bio-optical parameters from surface radiances (Siegel et al., 2002, Johannessen et al., 2003, Oliver et al., 2004). Unfortunately, the current discrete bands in the visible and near infra-red restrict the algorithm development to estimate chlorophyll-a, CDOM, and Kd490.

Recently, the hyperspectral imaging system has been implemented to the monitoring of land resources. Kerekes and Baum (2003) proposed the model for the hyperspectral imaging system to forecast remote sensing performance. The hyperspectral images were applied to many field of land remote sensing to identify and classify land objects (Mahesh and Mather, 2003, Haboudane et al., 2004, Thenkabail et al., 2004). Shafri et al. (2007) studied the performance of classification methods for the hyperspectral imaging data among the maximum likelihood

classification, the spectral angle mapper, the neural network, and the decision tree classifiers. Plaza (2006) discussed the possibility of the parallel processing for the hyperspectral imaging. These land applications are intended to classify targets and slightly different from the application in the oceanography.

In advance to the application of the hyperspectral sensor to the oceanography, the atmospheric correction was proposed with a spectrum-matching technique (Gao et al., 2000). Based on these studies, the ocean Portable Hyperspectral Image for Low-Light Spectroscopy (ocean PHILLS) was developed and demonstrated a good spectrum measurements as well as in-situ measurements (Davis et al., 2002). The hyperspectral sensors are applied to the coastal region to monitor the benthic habitats (Dierssen et al., 2003, Filippi et al., 2006), and to the coral reef (Mishra et al., 2007). In the oceanography, the coastal water is the strong interest to be studied, because of their sensitivity to the environmental change on the land and human activities like the dam construction in the upstream region of rivers. The coastal water should be analyzed from the remote sensor with discriminating substances in the water.

In this study, we discuss a possibility to estimate CDOM as the inherent optical properties as a function of the apparent optical properties from the hyperspectral imaging data. We introduce the in-situ measurements including CTD profiling, water sampling, and following water analysis, which are conducted simultaneously with the flight and measurements by the airborne hyperspectrum sensor near Japan.

2. METHOD FOR ALGORITHM DEVELOPMENT

2.1 CTD profiling with PAR sensor

The conductivity, temperature and depth sensors (CTD, RBR-420) with the photo-synthetically available radiation (PAR) sensor are deployed from a small boat to get the vertical profile of water temperature, salinity, and PAR. This profiler is operated in a logger mode, and data are retrieved after the cruise. The PAR sensor gives the downwelling irradiance integrated from 400 to 700 nm. The profiles given by CTD will provide us the basic physical concept of the water column.

2.2 Irradiance and radiance measurements with on-board spectrum meter

The spectrum irradiance and radiance radiometers (TRIOS) are operated to measure the downwelling irradiance and the surface upwelling radiance with the above water measurement protocol (Hooker and Lazin, 2000). The spectrum coverage of these radiometers are from 350 to 900 nm. Also, the spectrum irradiance radiometer is deployed into the water column to estimate the diffused attenuation coefficient ($K_d(\lambda)$) from the downwelling irradiance measurement at two different depths. The diffused attenuation coefficient at 490 nm is referred as one parameter to represent the concentration of suspended particles, which absorb and scatter the light penetration in the water column.

2.3 Water sampling

The surface water is sampled with a bucket sampling and the water near the bottom or at 10 m is sampled with the Niskin water sampler. The sampled water is analyzed to know the chlorophyll-a concentration, the nutrients concentration, the CDOM, and the suspended particles.

The chlorophyll-a concentration is determined by the fluorometric determination (Welschmeyer, 1994). The sampled sea water is filtered by the GF/F glass fiber filter. The GF/F filter is soaked with N, N-dimethylformamide for more than 24 hours. The fluorescence of the soaking liquid is measured by the Turner AU-10 to determine the chlorophyll-a concentration.

A large portion of the CDOM is considered as the terrestrially derived dissolved organic carbon that enters the ocean and some portion of the CDOM is from the fate of phytoplankton and zooplankton in the ocean. As the CDOM is defined by the spectrum absorption at 300 nm, the CDOM exhibits a distinct absorption at the ultra-violet (UV) spectrum. The UV light from the solar irradiation has a function to inhibit photosynthesis or to destroy the phytoplankton cell in the water. The UV penetration along the water column varies with the concentration of CDOM in the water. The sampled water is measured by the absorption spectrophotometer with 10 cm optical cell from 300 to 800 nm.

Suspended particles within the water are partly inorganic particles from river or ocean floor and organic particles from biogenic

activities in the ocean. The chemical composition of suspended particles vary and its optical properties also different in region. In this study, the sea water is filtered by the membran filter with a pore size of 0.2 μm and its dry weight is computed as the concentration of suspended particles in the unit volume. The concentration of suspended particles is compared with the diffused attenuation coefficient at 490 nm.

2.4 Hyperspectrum sensor measurements

The Airborne Imaging Spectrometer for Applications (AISA) is deployed synchronously with the in-situ measurement. The visible and near infrared sensor called Eagle and the short wave infrared sensor called Hawk are concurrently operated to get the surface radiance from 400 to 2400 nm with 190 channels.

The AISA data are processed for the atmospheric correction by the Fast Line-of-Sight Atmospheric Analysis of Spectral Hyercubes (FLAASH) to estimate the water leaving radiance.

3 DISCUSSION

The Sea Wide Field-of-View Sensor (SeaWiFS) and the Moderate Image Scanning Radiometer (MODIS), which have been used for ocean color monitoring, have the discrete spectrum bands, where a limited combination of spectrum bands are applied to estimate the concentrations of water substances. In contrast, the hyperspectrum sensor provides a continuous spectrum observation in all spectrum region with including a possibility to estimate geophysical parameters in different ways from the traditional ocean color algorithms.

Currently, the inherent optical properties like CDOM or $K_d(490)$ are estimated from the limited number of apparent optical properties. Johannessen et al. (2003) proposed the empirical equation to estimate the diffused attenuation coefficient at 323 nm, $K_d(323)$, as follows;

$$K_d(323) = 0.781 [R_{rs}(412)/R_{rs}(555)]^{-1.07} \quad (1)$$

where R_{rs} is the remote sensing reflectance that is given from the direct measurement of the remote sensor and the extraterrestrial solar irradiation. Then, the spectral absorption coefficient of CDOM, $a_{CDOM}(323)$, is given by;

$$a_{CDOM}(323) = 0.904 K_d(323) - 0.00714 \quad (2)$$

Similarly, $K_d(490)$ is given by the empirical equation (Mueller, 2000);

$$K_d(490) = 0.016 + 0.15645 [L_w(490)/L_w(555)]^{1.5401} \quad (3)$$

These estimates of inherent optical properties from the apparent optical properties have a freedom of 2 channels only.

In the hyperspectral remote sensing, we are able to increase the freedom of signal variation with more spectral bands. Fig. 1 shows the sample plots of three targets in 2007. One spectrum plot, showing a strong radiance in the near infra-red, is the upwelling radiance from the forest. Other two spectrum plots, exhibiting a low radiance in all spectrum range, are corresponding to the upwelling radiance from two different water mass.

We are currently, validating the hyperspectral data and in-situ data, and constructing a new algorithm to estimate an absorption coefficient for CDOM, a diffused attenuation coefficient of the water, and including chlorophyll-a concentration on the coastal waters.

The hyperspectrum remote sensing over the water is quite different from the target over lands, where the traditional classification does not work and it is required to classify the analogously distributed substances.

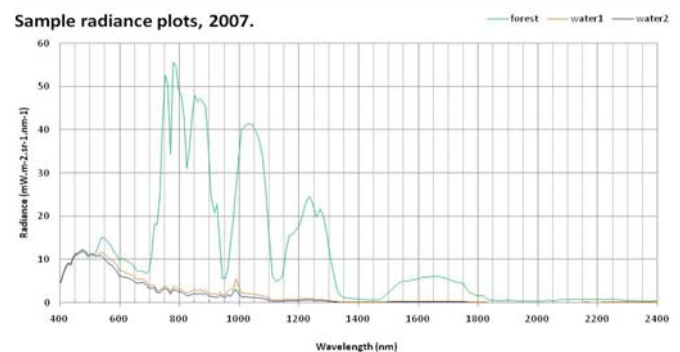


Fig. 1 Sample radiance plots from AISA 2007

REFERENCES

- Chami, M. (2007), Importance of the polarization in the retrieval of oceanic constituents from the remote sensing reflectance, *J. G. R.*, 112, C05026, doi:10.1029/2006JC003843.
- Davis, C. O., J. Bowles, R. A. Leathers, D. Korwan, T. V. Downes, W. A. Snyder, W. J.

- Rhea, W. Chen, J. Fisher, W. P. Bissett, and R. A. Reisse (2002), Ocean PHILLS hyperspectral imager: design, characterization, and calibration, *Optics Express*, 10 (4), 210-221.
- Dierssen H. M., R. C. Zimmerman, R. A. Leathers, T. V. Downes, and C. O. Davis (2003), Ocean color remote sensing of seagrass and bathymetry in the Bahamas Banks by high-resolution airborne imagery, *Limnol. Oceanogr.*, 48(1, part 2), 444-4555.
- Filippi, A. M., K. L. Carder, and C. O. Davis (2006), Vicarious calibration of the Ocean PHILLS hyperspectral sensor using a coastal tree-shadow method, *Geophys. Res. Lett.*, 33, L22605, doi:10.1029/2006GL027073.
- Gao, B. C., M. J. Montes, Z. Ahmad, and C. O. Davis (2000), Atmospheric correction algorithm for hyperspectral remote sensing of ocean color from space, *Applied Optics*, 39 (6), 887-896.
- Haboudane, D., J. R. Miller, E. Pattey, P. J. Zacro-Tejada, and I. Strachan (2004), Hyperspectral vegetation indices and novel algorithms for predicting green LAI of crop canopies: Modeling and validation in the context of precision agriculture, *Remote Sensing of Environment*, 90 (3): 337-352.
- Hooker, S. B., and G. Lazin (2000), The SeaBOARR-99 Field Campaign, SeaWiFS Postlaunch Technical Report Series, NASA Tech Memo 2000-206892, 8, 46pp.
- IOCCG (2000), Remote Sensing of Ocean Colour in Coastal, and Other Optically-Complex Waters, Ed. S. Sathyendranath, 140pp.
- Johannessen, S. C., W. L. Miller, and J. J. Cullen (2003), Calculation of UV attenuation and colored dissolved organic matter absorption spectra from measurements of ocean color, *J. Geophys. Res.* 108(C9), 3301, doi:10.1029/2000JC000514.
- Kerekes J. P. and J. E. Baum (2003), Hyperspectral Imaging System Modeling, *Lincoln Laboratory Journal*, 14, 1, 117-130.
- Mahesh, P. and P. M. Mather (2003), An assessment of the effectiveness of decision tree methods for land cover classification, *Remote Sensing of Environment*, 86, 554-565.
- Mishra, D. R., S. Narumalani, D. Rundquist, M. Lawson, and R. Perk (2007), Enhancing the detection and classification of coral reef and associated benthic habitats: A hyperspectral remote sensing approach, *J. Geophys. Res.*, 112, C08014, doi:10.1029/2006JC003892.
- Mueller, J. (2000), SeaWiFS Algorithm for the Diffuse Attenuation Coefficient, K(490), Using Water-Leaving Radiances at 490 and 555 nm, *NASA Technical Memorandum* 2000-206892, (11), 24-27.
- O'reilly, J. E., S. Maritorena, B. G. Mitchell, D. A. Siegel, K. L. Carder, S. A. Garver, M. Kahru, and C. McClain (1998), Ocean color chlorophyll algorithms for SeaWiFS, *J. Geophys. Res.*, 103, C11, 24,937-24,953.
- Oliver, M. J., O. Schofield, T. Bergmann, S. Glenn, C. Orrico. And M. Moline (2004), Deriving in situ phytoplankton absorption for bio-optical productivity models in turbid waters, *J. Geophys. Res.*, 109, C07S11, doi:10.1029/2002JC001627.
- Plaza, A. (2006), Parallel processing opens new perspectives for hyperspectral imaging, *SPIE Newsroom*, 10.1117/2.1200606.0275.
- Siegel, D. A., S. Maritorena, N. B. Nelson, D. A. Hansell, and M. Lorenzi-Kayser (2002), Global distribution and dynamics of colored dissolved and detrital organic materials, *J. Geophys. Res.*, 107(C12), 3228, doi:10.1029/2001JC000965.
- Shafri, H. Z. M., A. Suhaili, and S. Mansor (2007), The Performance of Maximum Likelihood, Spectral Angle Mapper, Neural Network and Decision Tree Classifiers in Hyperspectral Image Analysis, *J. Computer Science*, 3 (6): 419-423.
- Thenkabail, P. S., E. A. Enclona, M. S. Ashton, B. Van, D. Meer (2004), Accuracy assessments of hyperspectral waveband performance for vegetation analysis applications, *Remote Sensing of Environment*, 91 (3-4): 354-376.
- Wang, M., J. Tang, and W. Shi (2007), MODIS-derived ocean color products along the China east coastal region, *Geo. Res. Lett.*, 34, L06611, doi:10.1029/2006GL028599
- Welschmeyer, N. A. (1994), Fluorometric analysis of chlorophyll a in the presence of chlorophyll b and phaeopigments, *Limnol. Oceanogr.* 39, 1985-1992

Development of Mangrove Spectral Library

Hartanto Sanjaya, Ariani Andayani

Center for Natural Resources Inventory (TISDA), Agency for Assessment and Application of Technology (BPPT).
 Institute of Marine Research and Observation, Research Center for Marine Technology (PRTK), Agency for Marine and Fisheries Research (BRKP), Ministry of Marine Affairs and Fisheries

Development of mangrove spectral library

Hartanto Sanjaya, Center for Natural Resources Inventory (TISDA), Agency for Assessment and Application of Technology (BPPT).
 Ariani Andayani, Institute of Marine Research and Observation, Research Center for Marine Technology (PRTK), Agency for Marine and Fisheries Research (BRKP), Ministry of Marine Affairs and Fisheries
 Presented on APEC SAKE Workshop, Jakarta, 5 November 2007

Methods

- Study Site and Survey Design
- Mangrove Identification
- Field Data Acquisition (Measurement Procedure)

- Introduction
- Methods
 - Study Site, and Survey Design
 - Mangrove Identification
 - Field Data Acquisition
- Result
- References

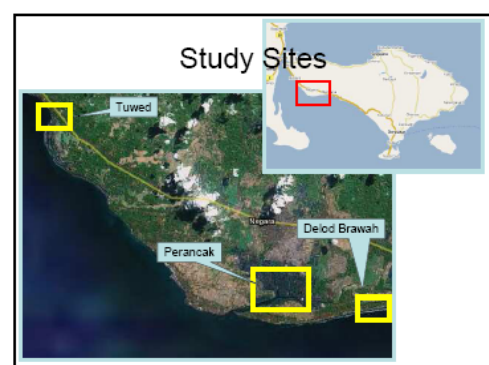
Method:

Study Sites and Survey Design

- In September of 2007 reflectance spectra were collected in Mangrove areas, Southern part of Kabupaten Jembrana, Bali:
 - Perancak
 - Delod Brawah
 - Tuwed

Introduction

- Spectral Library => finger print of objects => remote sensing data analysis.
- Mangroves => important plants in coastal zones.
- This study is to develop spectral library of Mangroves species.




Method: Survey Design

- Survey Design:
 - mangrove mapping (“roughly”)
 - identify the locations,
 - plan the optimum tracks
 - need special day(s)
 - Acquisition timing:
 - effective time range: 10am – 2pm
 - Number of days: depends

Method: Field Data Acquisition

- Reference and dark spectrum must be measured if at any time any sampling variable changes.
- In order to remove random noise from the spectral reflectance, the three spectra collected for each sample were averaged.



Method: Mangrove Identification

- “keys” to identify mangrove species:
 - Roots
 - Leaves
 - Flowers and Fruits
 - Tree’s shape
- Reference: Handbook of Mangroves


(in actions 😊...)



Tuwed, Jembrana, 2007

Mangrove Identification

Rhizophora apiculata



Tall-stilted Mangrove (Rhizophora apiculata)

This species is very similar to the Red Mangrove but has a less arborescent structure (it grows to 25 m tall).


Leaves: Pinnately. The species may be somewhat dark green the rest of other leaves of the same species track.

Leaves: Leaves are similar to those of the Red Mangrove. However, the leaves are pinnate, slightly longer and do not have brown stipules on the base.

Flowers and Fruits: Flowers are cream to light. Propagules similar to those of the Red Mangrove.

Bark: Rough, brown to dark grey-bark.

Stem: Species: The first Rhizophora (Rhizophora apiculata) and Rhizophora mucronata. The Red Mangrove has a long, slender, and has a lot of air.



Rhizophora mangle

Rhizophora apiculata


Marsh environment

Result

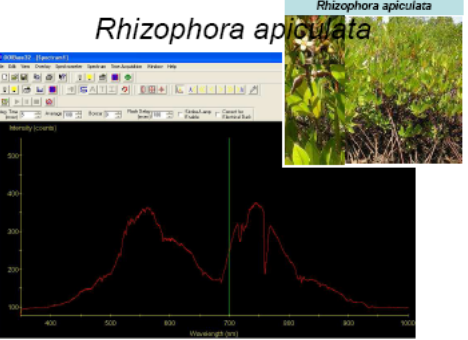
- Perancak Estuary (13 species):
 - *Acanthus ilicifolius*, *Aegiceras corniculatum*, *Avicennia alba*, *Avicennia marina*, *Bruguiera gymnorrhiza*, *Ceriops decandra*, *Hibiscus tiliaceus*, *Nypa fruticans*, *Sonneratia alba*, *Excoecaria agallocha*, *Xylocarpus granatum*, *Rhizophora stylosa*, *Rhizophora apiculata*
- Delod Brawah (2 species):
 - *Pandanus tectorius*, *Scaevola tacada*
- Tuwed (6 species):
 - *Ceriops decandra*, *Ceriops tagal*, *Spinifex littoreus*, *Osbornia octodonta*, *Sonneratia alba*, *Thespesia populnea*

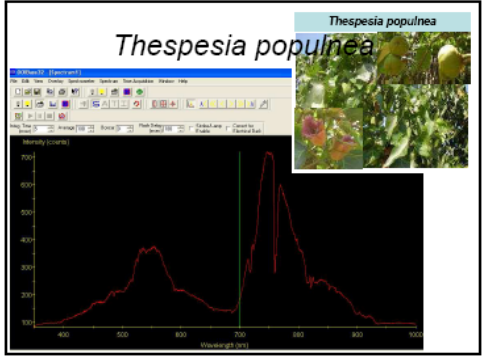
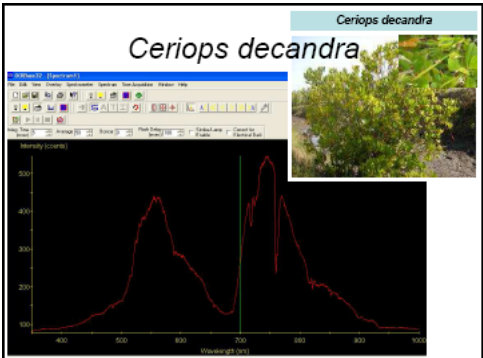
Method: Field Data Acquisition

- For each tree, 3 spectral measurements were taken of the sunlit side of the tree, at nadir from a distance of approximately 10 - 20 cm using a USB2000 Ocean Optics field spectrometer, equipped with a fiber optic cable of 1.5m.



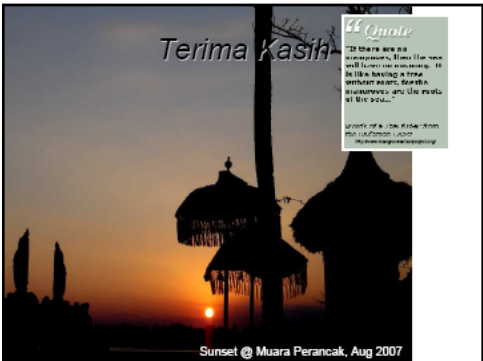
Rhizophora apiculata

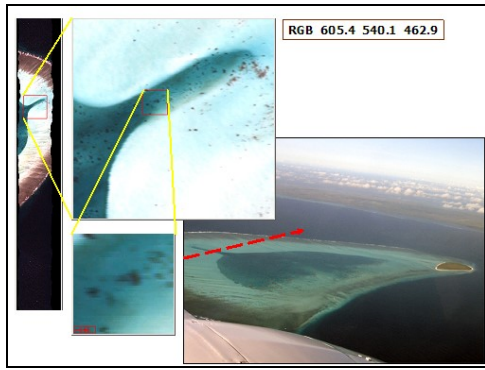




References

- Ferwerda, et.al., 2002, *Field Spectrometry of Leaves for Nutrient Assessment*, ITC The Netherland.
- Kitamura, Sozo et.al., 1997, *Handbook of Mangroves in Indonesia – Bali & Lombok*. Ministry of Forestry Indonesia, Japan International Cooperation Agency (JICA), The International Society of Mangrove Ecosystems (ISME), ISBN:4-906584-04-7.





The NDVI combination (R=NDVI, G=NDVI, B=NDVI) shows open areas (cyan) with colors ranging from orange to red, while red indicates location of shadow areas. Dark blue represents water and dark green/blue indicates cloud and its shadow. The green color indicates vegetation covered area. Within the vegetation area, also easily seen is the difference between mangrove along the coast and other vegetation types. This combination of NDVI is a good tool to (rapid) display and differentiate the various land cover types.

Comparing the PCA, NDVI with the classification result of PCA shows it generates the maximum likelihood method yields good land cover type identification. However, misclassification occurs over cloud and its shadow and also on the open water areas, which is classified to be along the entire coast of the island.

Comparing results of classification from PCA and that of BI and SAVI, the latter gives better result. It classified the village and cloud shadow areas better than getting PCA. Also vegetation types 1 and 2 are better separated. On the other hand, mangrove type is misclassified inside the island on several areas. The classification using BI and SAVI, in general gives consistent distribution of land cover types.

- Deep water
- Shallow water 1
- Shallow water 2
- Open land 1
- Open land 2
- Mangrove
- Vegetation 1
- Vegetation 2
- Vegetation 3
- Sand
- Residential

This study of Foradata Island use 2 types of images, hyperspectral CASI 550 (spatial resolution 2.5 m, 30 bands: 0.431-0.851 μm) and multispectral Terra-ASTER, acquired in 2003.

There was no detailed land cover data, so the classification analysis is based on pictures taken from aboard the survey boat, from the airplane while acquiring the hyperspectral data, and the socio-economic survey.

For this study, only one of the data strips was analyzed. It was chosen because it covers the various land cover types of Foradata Island. From the data strip, a subset of the region of interest was made (represented by red and yellow boxes). Preprocessing and atmospheric correction was conducted by VITO.

Conclusion

From the results of classifications between CASI and Terra-ASTER, it is obvious that CASI data is able to discriminate the various land cover types better than Terra-ASTER because of the finer spatial resolution and higher spectral resolution. Terra-ASTER is class on the other hand with wider spectral region is able to give good perspectives on general condition and land cover type of Foradata Island.

Acknowledgement

The Local Government of Maluku, Terngige Barat District for the cooperation in this project. The Belgian Science Policy Office for funding the Research Project and the Flemish Campaign for the Earth Remote Sensing Data Analysis Centre for providing the Terra-ASTER images.

A part of this presentation has been presented in the 3rd EARSEL Workshop on Imaging Spectroscopy, Brugge, Belgium, April 2007.

Two methods of classification were performed. The first classification is a supervised maximum likelihood. Principal component analysis was performed on the original 30 bands. The first 8 PCA were utilized and using 10 ROI (3 vegetation, mangrove, sand, 2 shallow water, deep water, 2 bare land) performed the maximum likelihood classification.

For the second classification, an MNP was performed, and then 3 general land cover types were extracted. They are open land, water and vegetation. On basis of the general land cover types, species level analysis was performed on the first 5 MNP with 4 ROI. On the general land cover of open land, there were 4 types of ROI (1 and open land 1 and 2, shallow water). On water, there were 4 ROI (shallow water, shallow water 1 and 2). And on the vegetation, there were also 4 ROI (mangrove, vegetation 1, 2, and 3). Then classification using spectral angle mapper was performed.

Comparing TCC and result of SAM, main misclassification occur over the shallow water region. Comparing between results of SAM and SAVI, the second classification method or SAM using MNP bands produce better result than the first in identifying land cover types in all three regions of water, open land, and vegetation.

Land Cover Types of Foradata Island using CASI Hyperspectral and TERRA-ASTER Data

Terra-ASTER's spectral resolution encompasses a wider spectral range than the CASI data (0.4164 - 0.8535 μm), namely the SWIR range of 0.85 - 11.65 μm. This enables the calculation of indices for vegetation (NDVI), water (NDWI) and soil (NDSI). With these indices, the false color composite of RGB = SVI or commonly called the NDVI may be produced.

For the classification of the land cover types the supervised maximum likelihood was employed. For the first classification, PCA of Terra-ASTER bands 1 through 9 were conducted and a supervised maximum likelihood classification of the first 3 PCA was performed using 11 regions of interest. The region of interests are 3 vegetation types, mangrove, shallow water, deep water, bare land, cloud shadow, sea grass, and residential.

The second classification method used is using images calculated for the Bottom Index (BI) and the Soil Adjusted Vegetation Index (SAVI). The Bottom Index is found by using the equation:

$$BI = \frac{R_1 - R_2}{R_1 + R_2 + 1}$$

where R_1 and R_2 are the reflectance of bands 1 and 2, k_1 and k_2 are the extinction coefficients of band 1 and band 2, respectively.

The SAVI was calculated with the following equation:

$$SAVI = \frac{1 - L}{1 + L} \left(\frac{R_3 - R_2}{R_3 + R_2 + 1} \right)$$

where L is the soil adjusted index (value of 0.5 is used), and R_3 and R_2 are reflectance of bands 3 and 2, respectively. Then supervised classification with maximum likelihood was performed on the Bottom Index and SAVI by using 11 ROI. These ROI are the same as the ones used for the first classification method.



Observations of SST and Chlorophyll-a Concentration in Coastal Sea of Vietnam Using Ocean Color Remote Sensing

Tu Tuyet Hong and Nguyen Phi Khu
University Technical Education -HCMC
Vietnam National University - HCMC

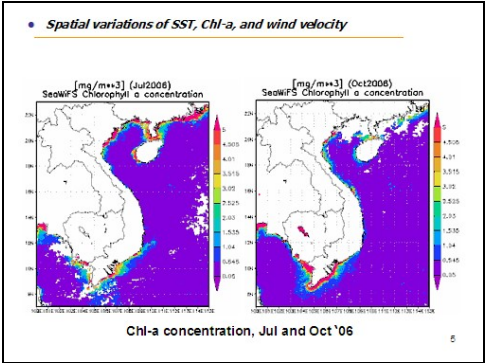
APEC – Marine Resource Conservation
THE 2nd SAKE WORKSHOP

SATELLITE APPLICATIONS TO
KNOWLEDGE-BASED ECONOMY

Observations of SST and chlorophyll-a
concentration in Coastal Sea of Vietnam
using ocean color remote sensing

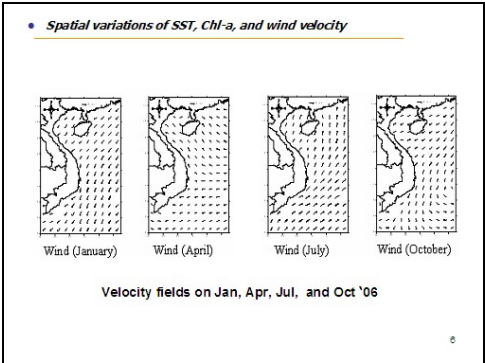
Tu Tuyet Hong - University Technical Education -HCMC
Nguyen Phi Khu - Vietnam National University - HCMC

2007
HO CHI MINH CITY - VIETNAM



Contents

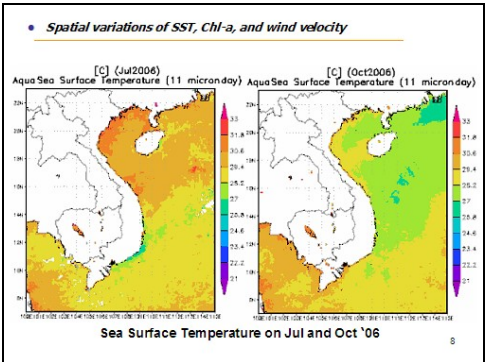
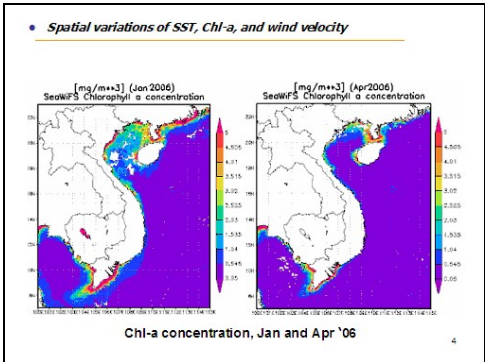
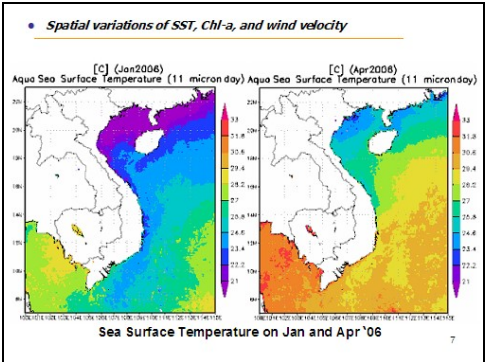
- Introduction
- Spatial variation of the Chl-a, SST, velocity in the study period
- Temporal variation of average monthly SST, Chl-a
- The relationship between Chl-a value and SST
- Conclusion



Data Sources

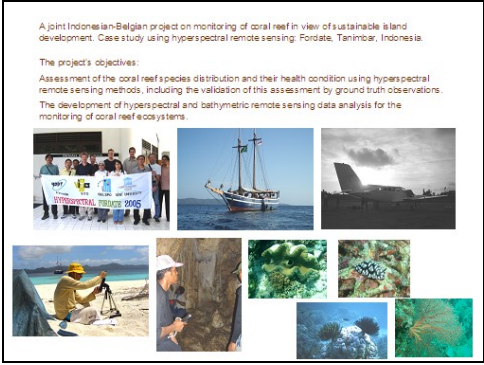
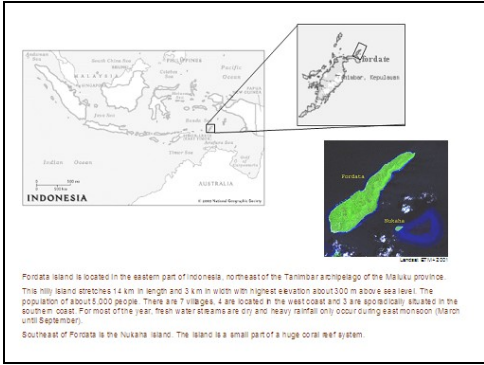
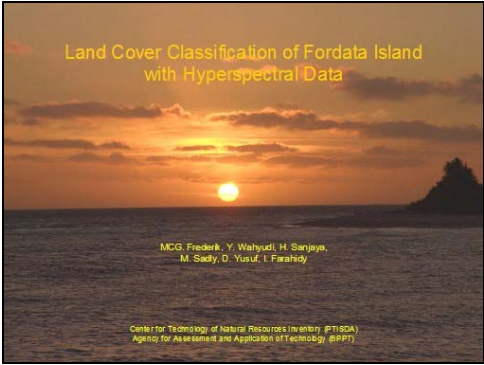
Case studies

- * Average monthly SST
<http://reason.gsfc.nasa.gov>
(SeaWiFS and Aqua-Modis)
- * Average monthly wind velocity
<ftp://ftp.ssmi.com>.
- * Field Obs. monthly
Provinces' Stations



Land Cover Classification of Fordata Island with Hyperspectral Data

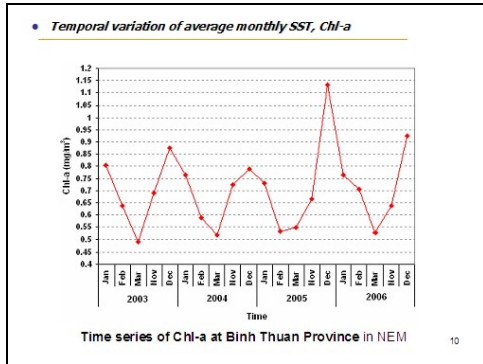
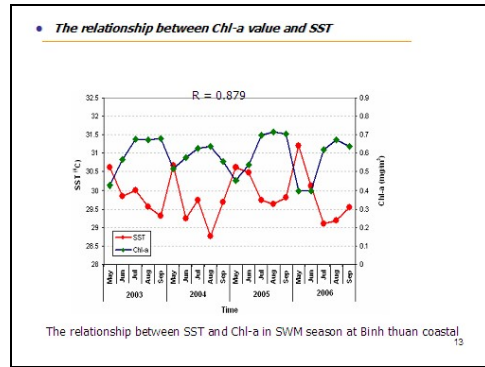
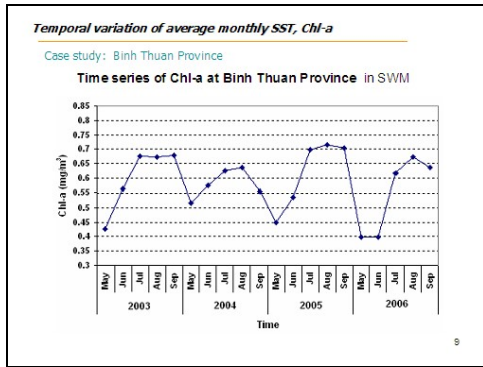
MCG, Frederik, Y. Wahyudi, H. Sanjaya, M. Sadly, D. Yusuf, I. Farahidy
 Center for Technology of Natural Resources Inventory (PTISDA)
 Agency for Assessment and Application of Technology (BPPT)



Aug 31 2006
 Project 1
 Location: 7°19' 27.5" S, 129° 5' 37.4" E
 Datasite: parks/keah/keah/keah

Picture	S	N	W	E	SW	SE	NE	EW	NS	SW	SE	NE	EW	NS	SW	SE	NE	EW	NS	SW	SE	NE	EW	NS	SW	SE	NE	EW	NS	SW	SE	NE	EW	NS	SW	SE	NE	EW		
1	50	50	50	50	50	50	50	50	50	50	50	50	50	50	50	50	50	50	50	50	50	50	50	50	50	50	50	50	50	50	50	50	50	50	50	50	50	50	50	50
2	50	50	50	50	50	50	50	50	50	50	50	50	50	50	50	50	50	50	50	50	50	50	50	50	50	50	50	50	50	50	50	50	50	50	50	50	50	50	50	50
3	50	50	50	50	50	50	50	50	50	50	50	50	50	50	50	50	50	50	50	50	50	50	50	50	50	50	50	50	50	50	50	50	50	50	50	50	50	50	50	50
4	50	50	50	50	50	50	50	50	50	50	50	50	50	50	50	50	50	50	50	50	50	50	50	50	50	50	50	50	50	50	50	50	50	50	50	50	50	50	50	50
5	50	50	50	50	50	50	50	50	50	50	50	50	50	50	50	50	50	50	50	50	50	50	50	50	50	50	50	50	50	50	50	50	50	50	50	50	50	50	50	50
6	50	50	50	50	50	50	50	50	50	50	50	50	50	50	50	50	50	50	50	50	50	50	50	50	50	50	50	50	50	50	50	50	50	50	50	50	50	50	50	50
7	50	50	50	50	50	50	50	50	50	50	50	50	50	50	50	50	50	50	50	50	50	50	50	50	50	50	50	50	50	50	50	50	50	50	50	50	50	50	50	50
8	50	50	50	50	50	50	50	50	50	50	50	50	50	50	50	50	50	50	50	50	50	50	50	50	50	50	50	50	50	50	50	50	50	50	50	50	50	50	50	50
9	50	50	50	50	50	50	50	50	50	50	50	50	50	50	50	50	50	50	50	50	50	50	50	50	50	50	50	50	50	50	50	50	50	50	50	50	50	50	50	50
10	50	50	50	50	50	50	50	50	50	50	50	50	50	50	50	50	50	50	50	50	50	50	50	50	50	50	50	50	50	50	50	50	50	50	50	50	50	50	50	50
11	50	50	50	50	50	50	50	50	50	50	50	50	50	50	50	50	50	50	50	50	50	50	50	50	50	50	50	50	50	50	50	50	50	50	50	50	50	50	50	50
12	50	50	50	50	50	50	50	50	50	50	50	50	50	50	50	50	50	50	50	50	50	50	50	50	50	50	50	50	50	50	50	50	50	50	50	50	50	50	50	50
13	50	50	50	50	50	50	50	50	50	50	50	50	50	50	50	50	50	50	50	50	50	50	50	50	50	50	50	50	50	50	50	50	50	50	50	50	50	50	50	50
14	50	50	50	50	50	50	50	50	50	50	50	50	50	50	50	50	50	50	50	50	50	50	50	50	50	50	50	50	50	50	50	50	50	50	50	50	50	50	50	50
15	50	50	50	50	50	50	50	50	50	50	50	50	50	50	50	50	50	50	50	50	50	50	50	50	50	50	50	50	50	50	50	50	50	50	50	50	50	50	50	50
16	50	50	50	50	50	50	50	50	50	50	50	50	50	50	50	50	50	50	50	50	50	50	50	50	50	50	50	50	50	50	50	50	50	50	50	50	50	50	50	50
17	50	50	50	50	50	50	50	50	50	50	50	50	50	50	50	50	50	50	50	50	50	50	50	50	50	50	50	50	50	50	50	50	50	50	50	50	50	50	50	50
18	50	50	50	50	50	50	50	50	50	50	50	50	50	50	50	50	50	50	50	50	50	50	50	50	50	50	50	50	50	50	50	50	50	50	50	50	50	50	50	50
19	50	50	50	50	50	50	50	50	50	50	50	50	50	50	50	50	50	50	50	50	50	50	50	50	50	50	50	50	50	50	50	50	50	50	50	50	50	50	50	50
20	50	50	50	50	50	50	50	50	50	50	50	50	50	50	50	50	50	50	50	50	50	50	50	50	50	50	50	50	50	50	50	50	50	50	50	50	50	50	50	50
21	50	50	50	50	50	50	50	50	50	50	50	50	50	50	50	50	50	50	50	50	50	50	50	50	50	50	50	50	50	50	50	50	50	50	50	50	50	50	50	50
22	50	50	50	50	50	50	50	50	50	50	50	50	50	50	50	50	50	50	50	50	50	50	50	50	50	50	50	50	50	50	50	50	50	50	50	50	50	50	50	50
23	50	50	50	50	50	50	50	50	50	50	50	50	50	50	50	50	50	50	50	50	50	50	50	50	50	50	50	50	50	50	50	50	50	50	50	50	50	50	50	50
24	50	50	50	50	50	50	50	50	50	50	50	50	50	50	50	50	50	50	50	50	50	50	50	50	50	50	50	50	50	50	50	50	50	50	50	50	50	50	50	50
25	50	50	50	50	50	50	50	50	50	50	50	50	50	50	50	50	50	50	50	50	50	50	50	50	50	50	50	50	50	50	50	50	50	50	50	50	50	50	50	50
26	50	50	50	50	50	50	50	50	50	50	50	50	50	50	50	50	50	50	50	50	50	50	50	50	50	50	50	50	50	50	50	50	50	50	50	50	50	50	50	50
27	50	50	50	50	50	50	50	50	50	50	50	50	50	50	50	50	50	50	50	50	50	50	50	50	50	50	50	50	50	50	50	50	50	50	50	50	50	50	50	50
28	50	50	50	50	50	50	50	50	50	50	50	50	50	50	50	50	50	50	50	50	50	50	50	50	50	50	50	50	50	50	50	50	50	50	50	50	50	50	50	50
29	50	50	50	50	50	50	50	50	50	50	50	50	50	50	50	50	50	50	50	50	50	50	50	50	50	50	50	50	50	50	50	50	50	50	50	50	50	50	50	50
30	50	50	50	50	50	50	50	50	50	50	50	50	50	50	50	50	50	50	50	50	50	50	50	50	50	50	50	50	50	50	50	50	50	50	50	50	50	50	50	50

There are a total of 30 transect lines collected



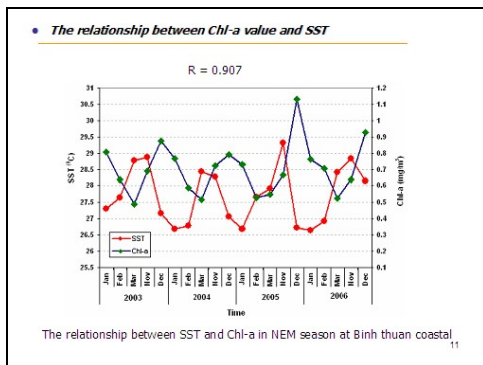
The relationship between Chl-a value and SST

	SST			
	2003	2004	2005	2006
Jan	27.303	26.680	26.685	26.651
Feb	27.651	26.777	27.638	26.935
Mar	28.766	28.440	27.936	28.401
Apr	30.359	29.988	29.762	30.483
May	30.611	30.665	30.615	31.208
Jun	29.838	29.254	30.468	30.117
Jul	30.014	29.741	29.737	29.110
Aug	29.574	28.768	29.632	29.190
Sep	29.323	29.683	29.822	29.553
Oct	29.007	29.028	29.798	29.335
Nov	28.871	28.280	29.318	28.841
Dec	27.160	27.068	26.733	28.158

Averaging area: lat=[7.0N,12.0N], lon=[100.0E,110.0E]

The relationship between SST and Chl-a in SWM season at Binh thuan coastal

14



- Recommendation**
- Spatial distribution features of SST and Chl-a in the Vietnam Sea depend up on: monsoons, precipitation, river runoff, upwelling, ect.
 - Temporal variation features of SST and Chl-a indicated that there are 4 seasons at Vietnam Sea: NE monsoon, Transition period from Spring to Summer, SW monsoon, and Transition period from Summer to Winter.
 - Along southern Vietnamese coast was formed a nearshore strip of low SST and high Chl-a during SW monsoon period.
 - Seasonal Chl-a variation in Vietnam waters is different between the north of Vietnam and south of Vietnam. The central of Vietnam waters is the lowest Chl-a concentration in both two seasons.
 - This study found that high Chl-a concentration at south of Vietnam waters from July to September during SWM (> 0.65 mg/m³).
- 15

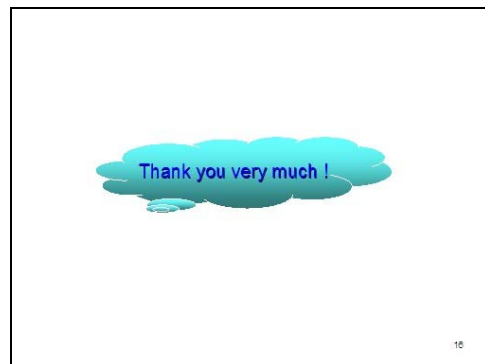
The relationship between Chl-a value and SST

	Chl-a			
	2003	2004	2005	2006
Jan	0.805956	0.764605	0.729043	0.764332
Feb	0.638264	0.589655	0.531317	0.707170
Mar	0.490380	0.517036	0.548989	0.526767
Apr	0.398628	0.400108	0.440129	0.388418
May	0.426313	0.516784	0.450032	0.398820
Jun	0.565014	0.575720	0.536319	0.398655
Jul	0.675098	0.625395	0.697992	0.617969
Aug	0.672159	0.636596	0.716033	0.672409
Sep	0.678790	0.556515	0.705443	0.638000
Oct	0.747492	0.673670	0.600371	0.697513
Nov	0.689427	0.723766	0.667040	0.638014
Dec	0.875886	0.790421	1.130850	0.926213

Selected averaging area: lat=[7.0N,12.0N], lon=[100.0E,110.0E]

The relationship between SST and Chl-a in NEM season at Binh thuan coastal

12



A Multi-Scale Detection Technique for Anomaly on Ocean Surface Using Optical Satellite Images

Chi-Farn Chen and Li-Yu Chang

Center for Space and Remote Sensing Research, National Central University, Chinese Taipei

ABSTRACT

Using satellite images for monitoring oceanic surface has become popular recently. One of the striking feature can be detected from satellite image is the anomalous phenomenon on oceanic surface. In general, it is easy to observe the diversified anomalies, caused by abrupt change of the reflectance on oceanic surface, on the optical satellite images. Among them, the anomaly caused by the pollution of oil spill or discharge of waste water is commonly observed. In this study, a multi-scale detection technique for studying anomaly on oceanic surface from optical satellite image is proposed. The study uses a RX algorithm at first to measure the degree of anomaly for each image pixel. Next, a series of Laplace of Gaussian operators at different scale are applied to extract the possible anomalous patches in different size. Finally, a threshold from the cumulative distribution of the RX algorithm's output is used to extract final anomalous patches. Experiment results show that the proposed method can extract striking anomalous patches at offshore or open water areas in different optical satellite images.

Keywords: Anomaly, Multi-Scale Detection, Satellite Images

1. INTRODUCTION

The radiant intensity at optical sensor is directly related to the reflectance of target. For anomalous targets on ocean surface, their reflectance usually varies a lot with respect the background. Therefore, the anomalous phenomena on ocean surface can be easily distinguished in optical sensors. In general, the causes to form different kinds of anomalies are diverse. The most common example is the anomaly causes by the pollution of oil spill (Brown and Fingas, 2001) or discharge of waste water (Keeler *et al.*, 2005). Theoretically, it is not difficult to develop an algorithm to extract those kinds of anomalies from images acquired from optical sensors. In fact, the reflectance responses for ocean surface and its related phenomena generally tend to be very low. This effect makes anomalies on ocean surface be affected by noise very easily. Especially for those anomalies have reflectance much lower than normal sea water. Consequently, it is not possible to set a clear threshold to extract anomalies form background.

2. METHODOLOGY

In this study, a multi-scale detection technique for anomaly on ocean surface from optical satellite image is proposed. The method can be divided into three sections: (1) A RX algorithm (Reed and Yu,

1990) is used at beginning to measure the degree of anomaly for each image pixel from multi-spectral satellite image. (2) For reducing the effect of noise, a series of Laplace of Gaussian operators (Pratt, 1991) at different scale are applied to extract the possible anomalous patches in different size. (3) A threshold from the cumulative distribution of the RX algorithm's output is used to extract final anomalous patches.

2.1 Measuring the degree of anomaly using RX algorithm

The RX algorithm shown in equation (1) actually is no more than a method to retrieve the normalized spectral distance for each pixel from multi-spectral image with respect to image mean.

$$\delta_{RXD}(r) = (r - \mu)^T K_{L^*L}^{-1} (r - \mu) \quad (1)$$

where

K : Covariance matrix of source image.

r : Spectral vector of each pixel.

μ : Image mean.

Originally, RX algorithm is also a method used to extract anomaly from remotely sensed images (Chang and Heinz, 2000). However, the most important assumption for using this algorithm is that the amount of anomalies should much less than the background. In fact, this assumption may

not be hold because we actually do not know how much less is the anomalies. In addition, a clear threshold has to be set in this algorithm. This is also not practical for the noisy nature of out data.

2.2 Filtering possible anomalous patches using Laplace of Gaussian operation

Generally speaking, the anomalies are the areas that greater than mean value in normalized distance image. On the other hand, the convex areas of normalized distance image may be potential areas of anomalies. For the purpose to detect convex areas, a second order derivative operator “Laplace of Gaussian” is introduced.

In fact, Laplace of Gaussian is the Laplace of a Gaussian smooth operator. Equation (2) is a 2 dimensional Gaussian smooth operator with standard deviation “s”. Equation (3) is the Laplace of Gaussian operator. Fig. 1 illustrates the pattern of Laplace of Gaussian operator.

$$G(x, y) = \frac{1}{\sqrt{2\pi s^2}} \exp\left(-\frac{x^2 + y^2}{2s^2}\right) \quad (2)$$

$$\nabla^2 G(x, y) = \frac{1}{\pi s^4} \left[1 - \frac{x^2 + y^2}{2s^2}\right] \cdot e^{-\frac{x^2 + y^2}{2s^2}} \quad (3)$$

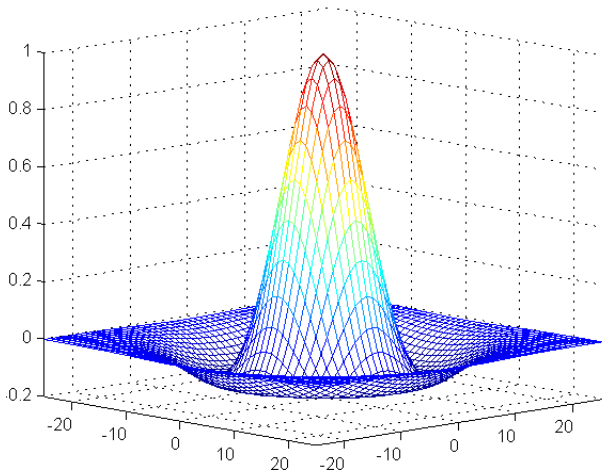


Fig. 1: The pattern of Laplace of Gaussian operator

Different scale of Laplace of Gaussian operator can be acquired by adjusting “s” parameters. The larger of “s” is used, the more smooth effect is achieved. Therefore, convex areas in different scales can be acquired by following procedure:

2.2.1.1 Convolving the normalized distance image with different scale of Laplace of Gaussian operator.

2.2.1.2 Taking positive part of the convolution output.

The following step in this section is to integrate those convex areas in different scales. In this study, we simply use “OR” operation to combine the entire convolution outputs at each scale. The reason that allows us to do this is the convex area in larger scale can always include the convex area in smaller scale. Therefore, after we use “OR” operation to combine all scale’s convolution outputs, the convex areas comes from different scales will be merged together.

2.3 Extracting anomalous patches using threshold

The convex areas in different scales acquired in last section are only potential anomalies. To finally conclude a convex area is an anomaly, we need to check the mean of normalized distance for all pixels in this patch. The selection of threshold used for assessing a patch is based on the cumulative distribution function of normalized distance. In this study, the threshold is set to the value that corresponding to 90% of cumulative distribution. A patch will be concluded as an anomaly if the patch mean is greater than threshold.

3 EXPERIMENTAL RESULTS

In this study, two experiments containing different characteristic of anomalies are test.

3.1 Case 1

In this case, the source image is SPOT-5 multi-spectral image. The image acquisition date was on 03/30/2006. The location is in south of Chinese Taipei. Fig. 2 shows the test image for this case. Notice that the anomalies in this dataset are darker than the background. Fig. 3 is the extracted anomalies using proposed scheme.

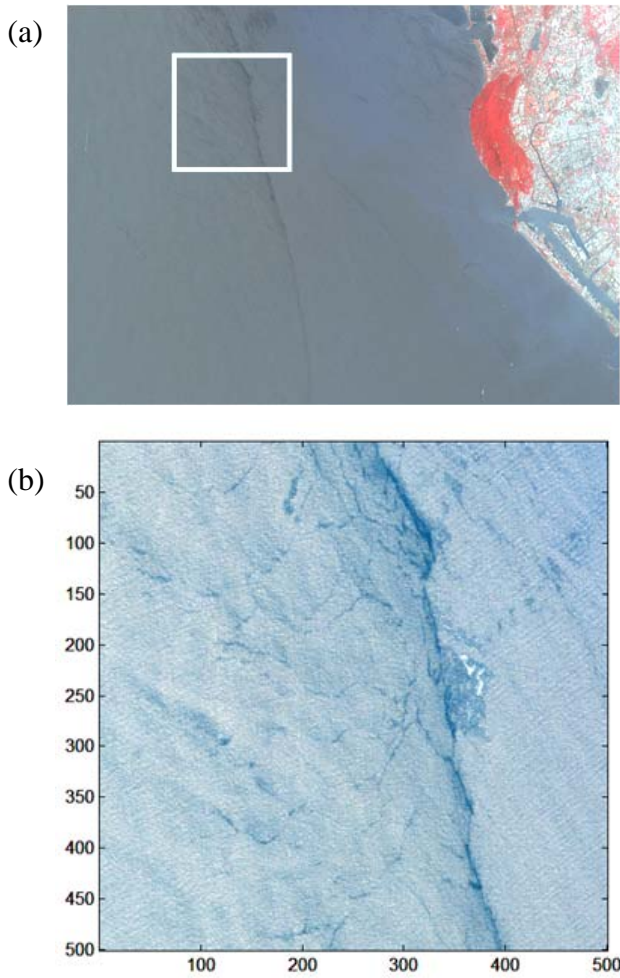


Fig. 2: The test image for case 1, (a) source image and study area for this case, (b) enlarged and enhanced image of study area.

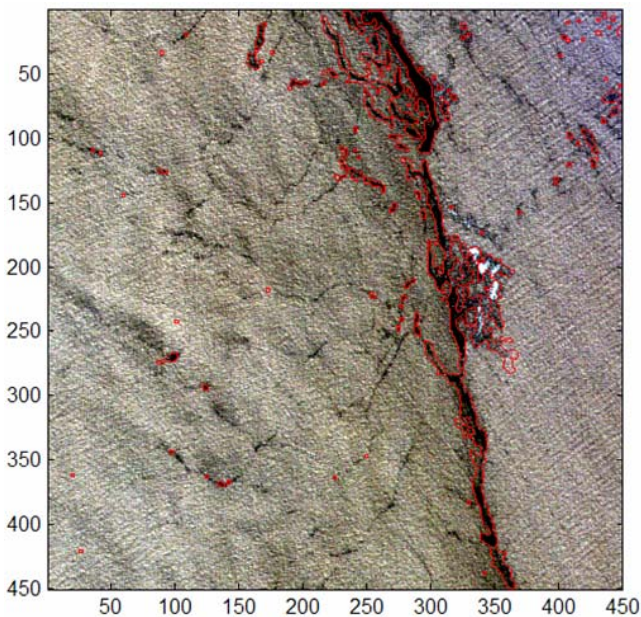


Fig. 3: The extracted anomalies overlay on source image

3.2 Case 2

In this case, the source image is also SPOT-5 multi-spectral image. The image acquisition date was on 07/18/2007. The location is in north of Chinese Taipei. Fig 4 shows the test image for this case. Notice that the anomalies in this dataset are brighter than the background. Fig. 5 is the extracted anomalies using proposed scheme.

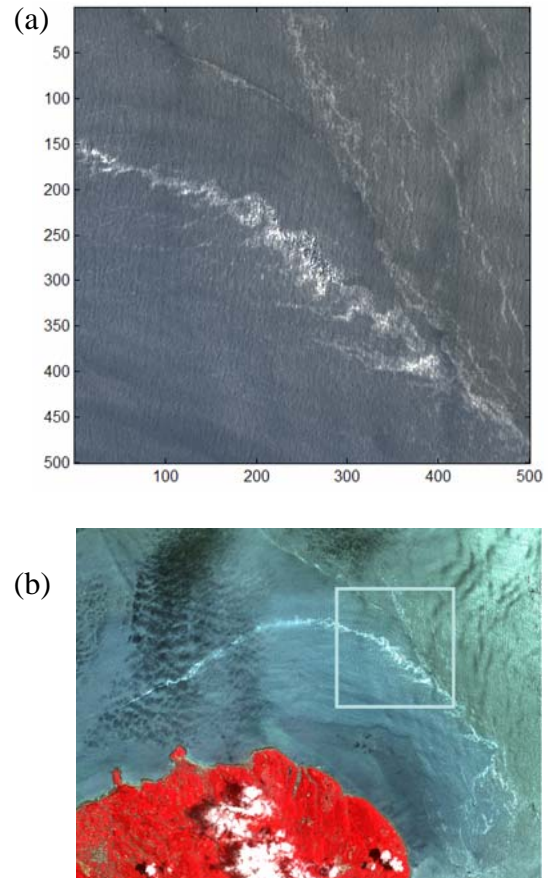


Fig. 4: The test image for case 2, (a) source image and study area for this case, (b) enlarged and enhanced image of study area.

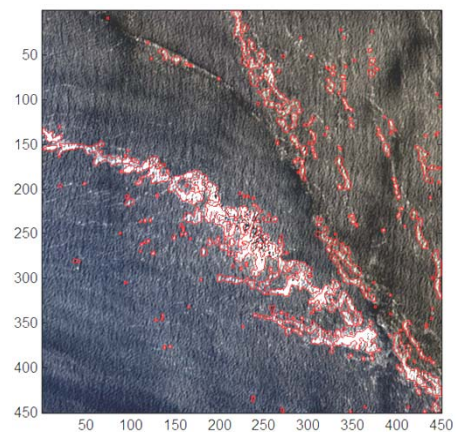


Fig. 5: The extracted anomalies overlay on source image

4. CONCLUSIONS

On ocean surface, the proposed scheme can successfully extract different kinds of anomalies using optical satellite images. Using RXD to retrieve normalized spectral distance enables that various kinds of anomalies can be extracted at the same time. With multi-scale Laplace of Gaussian operator, the noise is effectively reduced and the anomaly in different size can be separated to its corresponding scales for further processing.

The anomalies in larger scale tend to have a smoother boundary because of the stronger smooth effect introduced by large scale Laplace of Gaussian operator. Such problem may be solved by setting up a buffer zone along the boundary and using the anomalies detected in a smaller scale to replace those in this zone. This procedure can be used iteratively until the smallest scale is reached. The only fixed threshold used in proposed scheme is the normalized distance value at 90% of the cumulative distribution. A more adaptive way for estimating this threshold should be carried out to relax this limitation in future researches.

REFERENCES

- Brown CE, Fingas MF (2001) New space-borne sensors for oil spill response, Proceedings of International Oil Spill Conference 2001, Tampa, Florida: 911-916
- Keeler RN, Bondur VG, Gibson CH (2005) Optical satellite imagery detection of internal wave effects from a submerged turbulent outfall in the stratified ocean, Geophysical Research Letters, 32: L12610
- Reed IS, Yu X (1990) Adaptive multiple-band CFAR detection of an optical pattern with unknown spectral distribution, IEEE Transactions on Acoustic, Speech and Signal Processing, 38(10): 1760-1770
- Pratt WK (1991) Digital image processing, Wiley, New York
- Chang CI, Heinz D (2000) Constrained subpixel detection for remotely sensed images, IEEE Transactions on Geoscience and Remote Sensing, 38(3): 1144-1159

Simulation of Spilled Oil in Seribu Islands Waters

Safwan Hadi^{1,2}, Totok Suprijo¹, Haris Sunendar²
 1 Resarch Group of Oceanography, ITB
 2 Center for Marine and Coastal Development, ITB



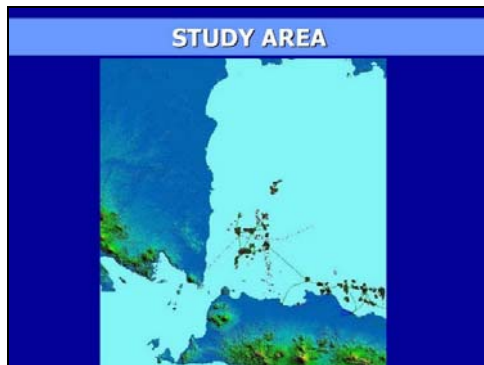
GOVERNING EQUATIONS

Continuity Equation:

$$\frac{\partial \zeta}{\partial t} + \frac{\partial U}{\partial x} + \frac{\partial V}{\partial y} = 0$$

Momentum Equation:

$$\frac{\partial U}{\partial t} + U \frac{\partial U}{\partial x} + V \frac{\partial U}{\partial y} + gH \frac{\partial \zeta}{\partial x} + fU \frac{\sqrt{U^2 + V^2}}{H} + A_{ed} \Delta_h^2 U = \lambda W_x \sqrt{W_x^2 + W_y^2}$$

$$\frac{\partial V}{\partial t} + U \frac{\partial V}{\partial x} + V \frac{\partial V}{\partial y} + gH \frac{\partial \zeta}{\partial y} + fV \frac{\sqrt{U^2 + V^2}}{H} + A_{ed} \Delta_h^2 V = \lambda W_y \sqrt{W_x^2 + W_y^2}$$


TRAJECTORY EQUATIONS

Trajectory Equation Caused by Wind and Current

$$XPW(m, n)^{t+\Delta t} = XPW(m, n)^t + \Delta t (U_x^{t+\Delta t} + 0.03 U_w + (\mu - 0.5) P_u)$$

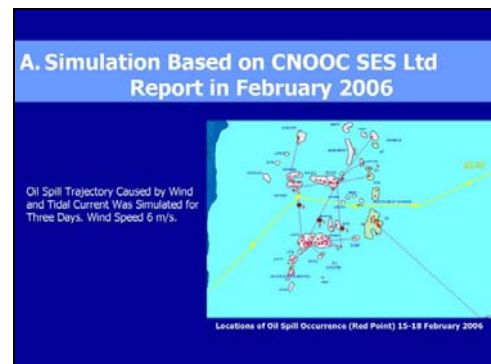
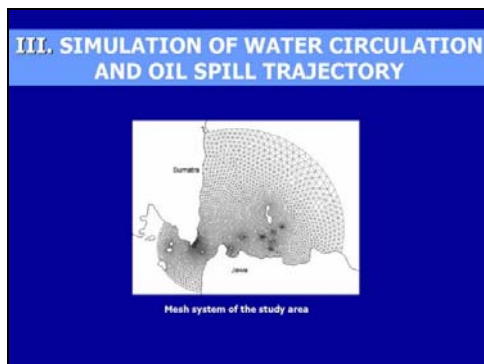
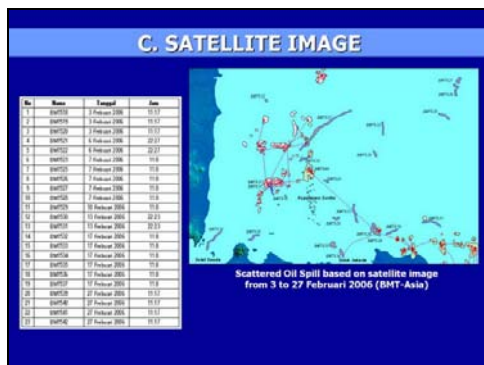
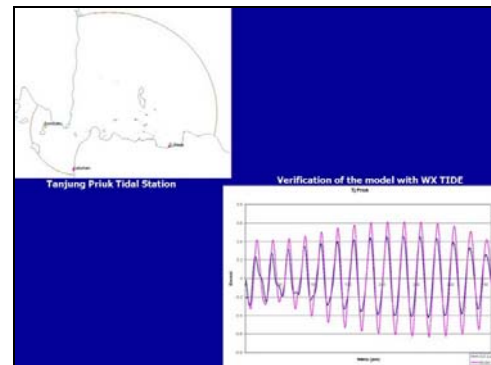
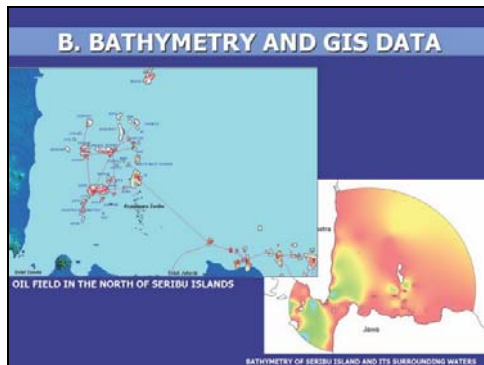
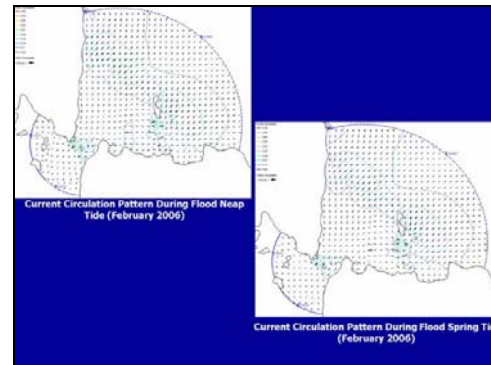
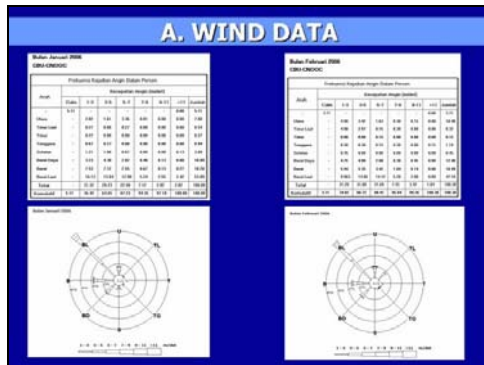
$$YPW(m, n)^{t+\Delta t} = YPW(m, n)^t + \Delta t (V_y^{t+\Delta t} + 0.03 V_w + (\mu - 0.5) P_v)$$

I. OBJECTIVE OF THE STUDY

1. To Develop Oil Spill Model For Seribu Islands Waters – North Of Jakarta.
2. To Use The Model to Predict The Movement of Spilled Oil from Oil Field in the North Of Seribu Islands.

II. DATA USED FOR THE SIMULATION


- A. WIND DATA
- B. BATHYMETRY AND GIS DATA
- C. SATELLITE IMAGE



B. Simulation Based on Interpretation of Satellite Image

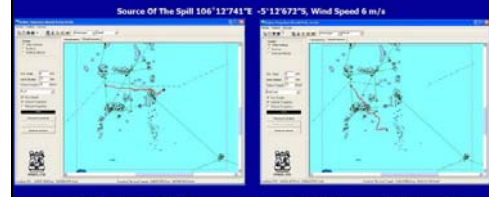
Analysis of Oil Spill Occurrence Based on RADARSAT Image – 1 Wide Beam 3 by BMT – Asia Pacific PTE Ltd for CNOOC SES Ltd, February 2006.

There Were 23 Oil Spill Occurrences During February 2006.



Scattered Oil Spill based on satellite image from 3 to 27 February 2006 (BMT-Asia)

Source Of The Spill 106°12'741"E -5°12'672"S, Wind Speed 6 m/s



Simulation for 72 hours, Wind from West, Travelling Distance 46327.06 meter

Simulation for 72 hours, Wind from NorthWest, Travelling Distance 44859.21 meter

C. Trace Back Simulation Based on Spilled Oil Found in Bira Island (Seasonal Variation)

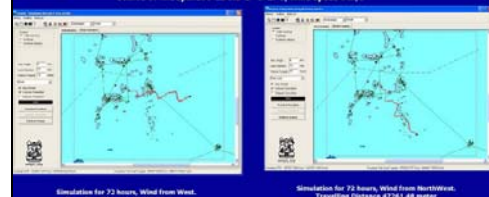
Trace Back Simulation From Bira Island With Wind Data From CBU for 240 Hours From February 19 2006

D. Simulation Based on Observed Daily Wind Data at CBU Station.

Based on the Fact Found in The Field There Are Two Patterns of Oil Spill Occured in Seribu Islands :

- East Monsoon → Spilled Oil Found Around Pramuka Island
- West Monsoon → Spilled Oil Found Around Bira Island

Source Of The Spill 106°13'5.5"E -5°17'S, Wind Speed 6 m/s



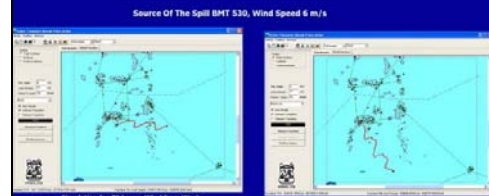
Simulation for 72 hours, Wind from West, Travelling Distance 45297.08 meter

Simulation for 72 hours, Wind from NorthWest, Travelling Distance 47251.48 meter

RESULTS OF OIL SPILL SIMULATION

B. Simulation Based on Interpretation of Satellite Image

Source Of The Spill BMT 530, Wind Speed 6 m/s




Simulation for 72 hours, Wind from West, Travelling Distance 46441.89 meter

Simulation for 72 hours, Wind from NorthWest, Travelling Distance 46752.02 meter

A. Simulation Based on CNOOC SES Ltd Report in February 2006

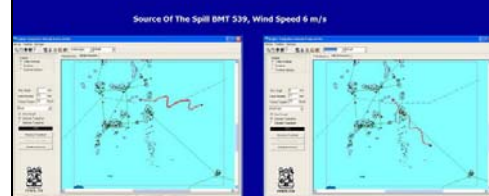
Source Of The Spill 106°13'285"E -5°12'541"S, Wind Speed 6 m/s



Simulation for 72 hours, Wind from West, Travelling Distance 47894.74 meter

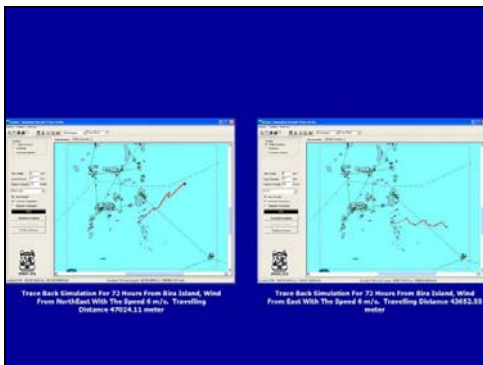
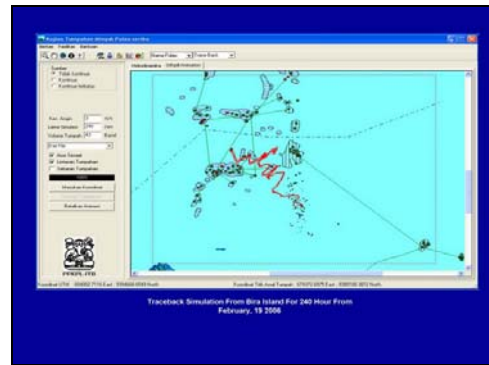
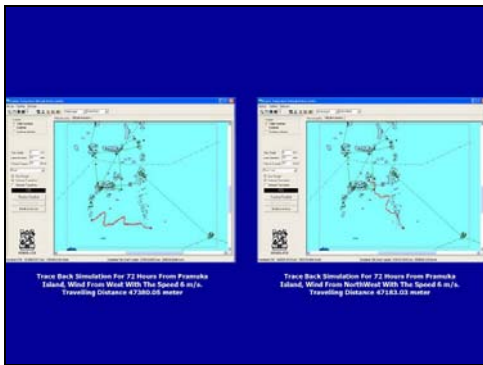
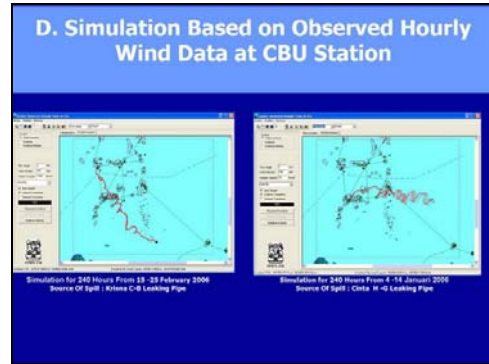
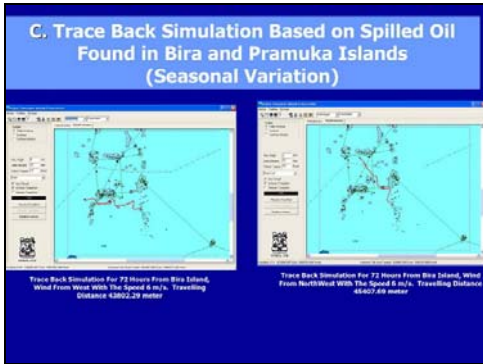
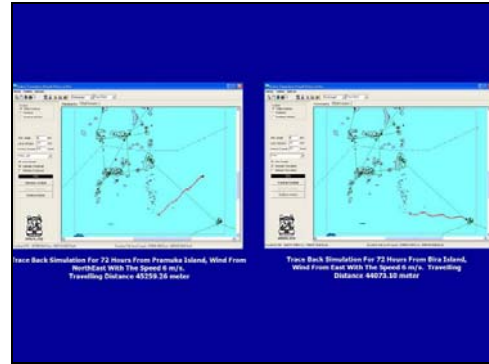
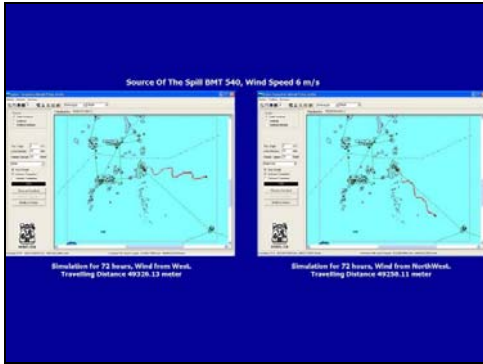
Simulation for 72 hours, Wind from NorthWest, Travelling Distance 46402.33 meter

Source Of The Spill BMT 539, Wind Speed 6 m/s



Simulation for 72 hours, Wind from West, Travelling Distance 46630.72 meter

Simulation for 72 hours, Wind from NorthWest, Travelling Distance 46136.21 meter



IV. CONCLUSION

1. Oil Spill Model Develop in The Study Show Good Capability of Simulating Oil Spill Trajectory in Seribu Islands Water.
2. Oil Platform Situated in the North of Seribu Islands are Potential threat for Oil Pollution in Seribu Islands.
3. Local Government of Seribu Islands Should Develop Mitigation Plan to Reduce the Risk of Oil Pollution in Seribu Islands in The Future.

Identification of Groundtruthing Needs for The Extended Use of Satellite Imagery in Nearshore Habitat Mapping

Karen v. Juterzenka

*Department of Marine Science and Technology, Bogor Agricultural University, Indonesia
Email: kvjuterzenka@hazweio.com*

Satellite applications have gained more and more significance in marine research as well as for management purposes.

Detailed and sound habitat classification and habitat mapping is one of the pre-requisites for qualified decisions in marine resource planning and conservation. Satellite imagery contributes substantially to the mapping of coastal and nearshore ecosystems, but is still limited by the restriction in dimensions – for waters exceeding the coastal strip - and the spatial resolution. In the past, restrictions of satellite imaging methods had led to some disappointments by ecologists and resource managers regarding its application in research and coastal zone management. New sensors had been developed in the meantime - however, possibly more insights in nearshore habitat details and distribution can be obtained by a closer coupling of satellite imagery and an improved strategy of three-dimensional ecological groundtruthing.

This paper shall contribute to the discussion about groundtruthing needs for coastal and neritic habitat mapping and management purposes by addressing recent examples including Indonesian waters.

To put it short: Some marine ecologists and biological oceanographers are still not very happy about the results they can achieve from satellite imagery – despite promising cover and improved resolution, they may fail in providing „hard“ data in the long run. Ten years ago, Mumby and coworkers proposed the use of airborne digital photography (Mumby et al. 1998) for reef studies, and airborne 3d measurements can reveal terrestrial canopy structure with a spatial resolution of 1-10 m. But even if satellite and airborne sensors and resolution are appropriate, a reliable classification system is needed, e.g. to distinguish corals reefs from seagrass beds and defining habitat borders for management purposes. The borders as well as hot spots and weak spots in terms of biodiversity and ecosystem function are most important to detect and monitor environmental changes and habitat loss (Kerr & Ostrovsky 2003). Spatial resolution „as

such“ seems not a problem any more, at least concerning the cover of terrestrial and most coastal ecosystems (Turner et al. 2003) as well as man-made (well-defined) structures (Kam et al 2006). As an expression of widespread needs, a minisymposium in the framework of The International Coral Reef Symposium 2008 will cover emerging techniques in remote sensing, also dealing with the question „What types of benthic information can be obtained from remote observation?“ From the perspective of a benthic ecologist and a biological oceanographer there might be another point of view – what can benthic ecology contribute to gain optimal information from remote sensing methods. Earth observation systems already provide the majority of spatial-temporal information on habitat extends, which is needed for coastal management purposes, and new sensor developments always try to bridge actual information gaps (Navalgund & Jayanthi). Probably some gaps can also be filled by approaching the problem from the benthic side, if you cannot see all details from above.

Ecologists as well as managers complain that field and remote sensing data are often collected at divergent spatial scales. The issues might be solved by intensified exchange between remote sensing specialists and field scientists prior to the implementation of field assessment campaigns. Moreover, satellite imaging enables the scientists to identify and set preliminary limits to sensitive areas, which might suffer degradation or damage in the future, and to include this information in the design of ocean-based monitoring and groundtruthing programs before serious changes in habitat extent or habitat structure occur. This might help (1) to extract more valuable information from temporal satellite image series and (2) to improve existing classification systems by identifying the dynamics of marine communities at the ill-defined transition zones between habitats.

Thus, transdisciplinary approaches of remote sensing specialists and marine ecologists might be seen as an integrated tool to extract information about marine community structure down to species level, as well as the functioning of marine systems, from satellite information.

REFERENCES

- Kam, S.P., Liew, S.C., Muchlisin, Z.A., Chen. P. (2006) Remote sensing and field assessment of Tsunami effects on coastal pond aquaculture in Northern Sumatra. NAGA Worldfis Center Quaterly, 29: 4-9
- Kerr, J.T., Ostrovsky, M. (2003) from space to species: ecological applications for remote sensing. TREE 18: 299-305
- Mumby P.J., Green, E.P., Clark, C.D., Edwards, A.J. (1998) Digital analysis of multispectral airborne imagery of coral reefs. Coral Reefs 17: 59-69
- Navalgund, R.R., Jayanthi, S.C. (2002) Role of Earth Observations for Sustainable Development: Emerging Trends. Paper/ICORSE Earth Observation Systems for Sustainable Development
- Turner. W., Spector, S., Gardiner, N., Fladeland, M., Sterling. E., Steininger, M. (2003) Remote sensing for biodiversity and conservation. TREE 18: 306-314

Formosat-2 Satellite Imagery Assessment for Coastal Ecosystem Mapping in Western Coast of Banten, Indonesia

Syamsul B. Agus¹ and Indra Pratama²

*¹ Department of Marine Science and Technology, Bogor Agricultural University
² Agency for Marine and Fishery Research, Ministry of Marine Affairs and Fisheries*

ABSTRACT

Coastal ecosystems in West Banten are valuable, providing products and services for the livelihood of its community, and highly threatened. Threats facing coastal ecosystems in West Banten are rapid growth of coastal populations, increasing exploitation of coastal resources, alteration and loss of habitats, also high runoff carrying sediment and other terrestrial-based pollutants from coastal rivers. Mapping of coastal ecosystems will provide significant baseline data for future monitoring and sustainable management of coastal ecosystems in West Banten. Using FORMOSAT-2 data obtained on August 9, 2007, we assess current condition of coastal ecosystems in West Banten area on August 9-11, 2007. Using both data from FORMOSAT-2 satellite imagery and from field assessment, with this paper we exposed map featuring six class of coastal cover-area in West Banten. This study also measured spectral reflectance from 24 objects in West Coast of Banten.

Keywords: FORMOSAT-2, coastal, map, Banten

1. INTRODUCTION

Most of border area in Banten Province, located in 5° 7' 50" - 7° 1' 11" S and 105° 1' 11" - 106° 7' 12" E, represent coastal environment with complex use of its resources (DEPKIMPRASWIL 2003). West Coast of Banten bordering with the Sunda Strait is subject to marine tourism, transportation, industry, fisheries, and conservation. Up to this day a great variety of human activities happen there simultaneously. The main environmental impacts consist of alteration and loss of coastal habitats due to resource exploitation and development, organic and inorganic pollution, volcanic eruption from the Krakatau, and tsunami. Scientific data on coastal ecosystems, land use, landforms, and shoreline and water quality are required periodically to ensure an environmentally effective coastal zone management practices. Maps on various coastal themes form basic input to the coastal zone management models. Conventional maps are quite useful; however, they do not provide up-to-date information. Since coastal zone is very dynamic, periodic mapping is vital for planning effective strategies.

The interpretation of remotely sensed data is the best tool currently available for providing synoptic spatial information on various scales and with reasonable classification and control accuracy. The availability of FORMOSAT-2, which

produced hyperspectral data with spatial resolution of 8 m for multispectral and 2 m for panchromatic images, is expected to provide spatially comprehensive coverage at a higher resolution for effective and accurate analyses of different coastal ecosystems exist within one area. There are five spectral bands in FORMOSAT-2, i.e. P: 0,45–0,90 μ m (panchromatic), B1: 0,45–0,52 μ m (blue), B2: 0,52–0,60 μ m (green), B3: 0,63–0,69 μ m (red), and B4: 0,76–0,90 μ m (near-infrared). The objective of this research is to test the ability of FORMOSAT-2 data in producing coastal geospatial data, particularly for mapping of coastal ecosystems, i.e. mangrove forests, seagrass beds, and coral reefs, in West Banten area.

2. METHODS

2.1 Study sites

This study was conducted on August 5-7, 2007, in coastal area of West Banten, with geographic reference of 6° 15' 40" - 6° 41' 30" S and 105° 35' 00" - 106° 00' 00" E. West Banten coastal platform extends north-south, bordered with Sunda Strait and is influenced by volcanism activities from Mount Krakatau. Thus, its shorelines and living coral communities were geologically incipient (Tomascik et al 1997). There were two small islands located near the coasts of West Banten, i.e. Popoleh Island and

Karang Gosong Island. There were 22 study sites, particularly to obtain seawater samples, including 3 sites for coral assessment and 1 site for mangroves and seagrass assessment (Figure 1).

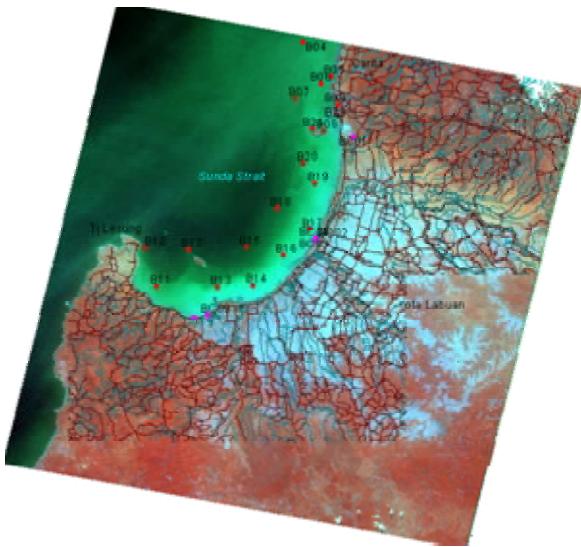


Figure 1. Study sites

2.2 In-situ sampling

In general, *in-situ* sampling conducted comprises of coastal ecosystem assessment and spectroradiometric measurements of sediment types and species. Assessed coastal ecosystems were mangroves, seagrass beds, and coral reefs, which techniques were based on English et al (1997). Reflectance measurements were made to create a spectral library of 24 reflectance spectra encompassing mangroves, other coastal vegetation, fishponds, several types of coastal-substrates and different colors of seawater.

2.3 Satellite image analysis

Morphologies of the beaches, lagoons, mangrove forests, seagrass beds, and coral reefs were classified on the basis of the spectral signatures of their various habitats using images produced from FORMOSAT-2 satellite image obtained on August 9, 2007. Geometric correction was trained with existing ground-truth data and reference map from BAKOSURTANAL were performed using ER Mapper and Arc View (Green et al. 2000).

3. RESULTS AND DISCUSSION

3.1 FORMOSAT imagery

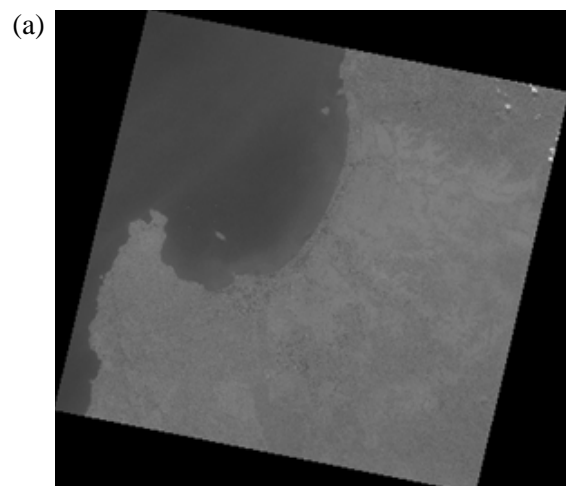
The main remote sensing mission for FORMOSAT-2, which was launched in 2004, was to capture satellite images of the Taiwan Island and the surrounding islands and ocean to monitor the environment and its resources. Later on, under international collaborative agreement, FORMOSAT-2 was also used to capture images of other regions in the Asia Pacific. Within the frame of APEC SAKE on Satellite Application on Fishery and Coastal Ecosystem (SAFE), FORMOSAT-2 acquires capture satellite images of Indonesian coastal and archipelagic waters (Figure 2).



Figure 2. Satellite images of West Banten produced by FORMOSAT-2,

- = acquisition date July 7, 2006 and
- = acquisition date August 9, 2007.

On July 7, 2006, FORMOSAT-2 captured the first satellite image of West Banten. Due to stripping error, the images were incapable for further processing. One year later, FORMOSAT-2 acquires another image of West Banten on August 9, 2007. Panchromatic FORMOSAT-2 images of West Banten are presented in Figure 3, while multispectral FORMOSAT-2 images of West Banten are presented in Figure 4.



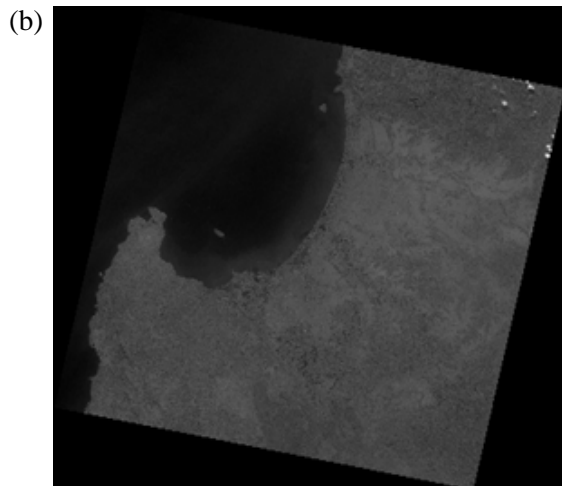


Figure 3. Panchromatic FORMOSAT-2 image of West Banten, (a) prior to geometric correction and (b) after geometric correction.

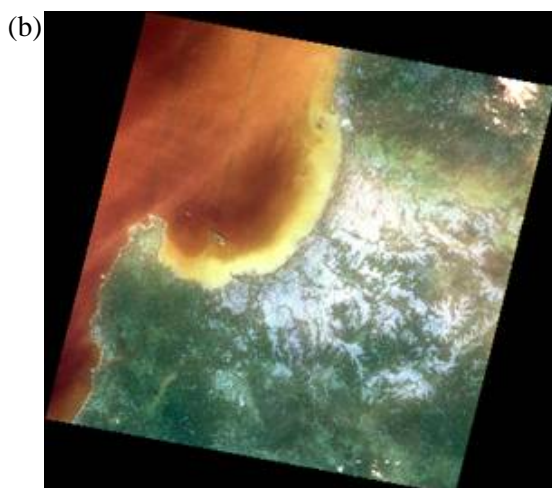
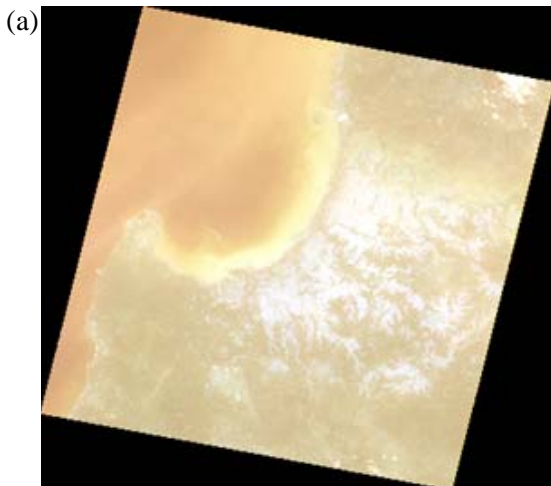


Figure 4. Multispectral FORMOSAT-2 image of West Banten, (a) prior to geometric correction and (b) after geometric correction.

3.2 Coastal ecosystems of West Banten

Coral communities in West Banten are influenced by volcanism and extreme sedimentation due to lots of river discharges, thus resulting in patchy distribution and no significant carbonate accretion to form fringing reefs as if before 1883 Krakatau eruption (Tomascik 1997). From three observed sites, i.e. Popoleh Island, Karang Gundul, and Karang Gosong, the highest cover of hard corals were available in Karang Gundul (43.0%). Benthic communities in Popoleh Island were dominated by soft corals of *Lobophytum*, while calcareous macroalgae of *Halimeda* were common in Karang Gosong (Figure 5). Common Scleractinian corals observed were *Acropora*, *Pocillopora*, *Stylophora*, *Porites*, *Favia*, and *Montipora*.

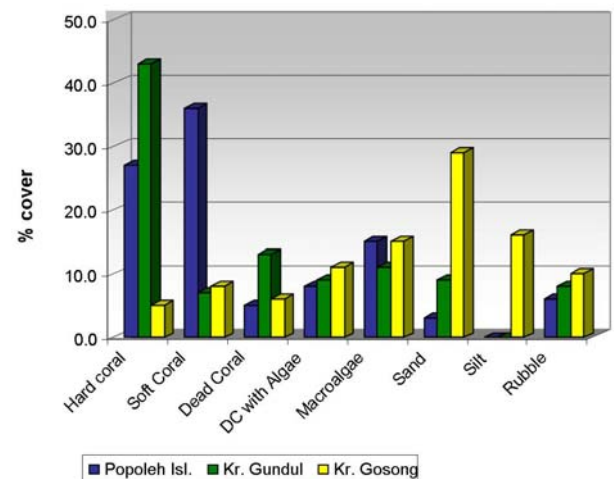


Figure 5. Results of coral reef assessment in West Banten

There was only one species of seagrass observed in the study sites, *Enhalus acoroides*, which is the largest species of seagrass. In relation to general feature of study sites, existing silty to muddy sediments support *Enhalus* to form monospecific meadows. Mangrove vegetation in study sites comprised mainly of *Rhizophora* and *Bruguiera*. Other mangrove species observed in the surroundings were *Avicennia*, *Sonneratia*, *Xylocarpus*, *Ceriops*, and *Exoecaria*.

High resolution (8 m) classification map was generated for coastal environment of West Banten, Indonesia, from a mosaic of FORMOSAT-2 multispectral images to produce six classes (Figure 6). Contrast-stretched, multi-spectral image maps provided a qualitative method to distinguish different types of seawater (deep, shallow, and high turbid waters), mangrove forests, bushes and

other coastal land-vegetation, also rice fields and housings. This map, in a geographic information system (GIS) format, can be used for fieldwork, as base maps for other scientific studies and for management of coral reef ecosystem.

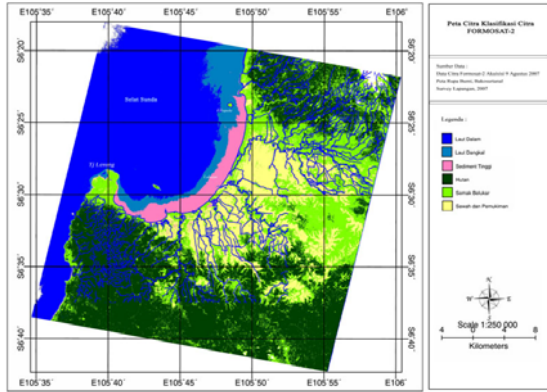
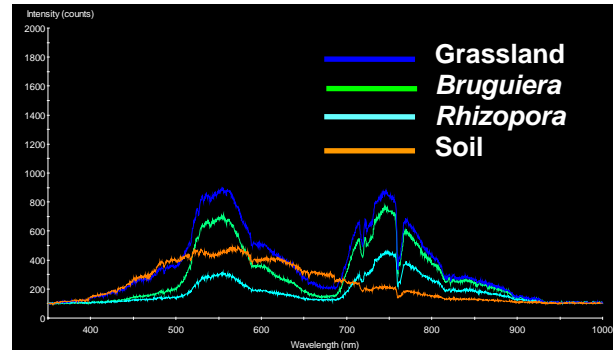


Figure 6. Classified map of coastal environment in West Banten, using multispectral FORMOSAT-2 image with spatial resolution of 8 m.

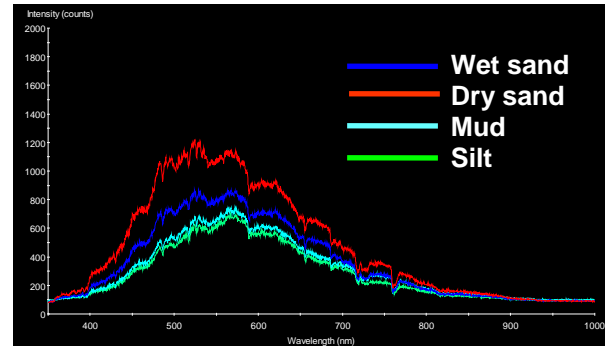
High resolution (8 m) classification map was generated for coastal environment of West Banten, Indonesia, from a mosaic of FORMOSAT-2 multispectral images to produce six classes (Figure 6). Contrast-stretched, multi-spectral image maps provided a qualitative method to distinguish different types of seawater (deep, shallow, and high turbid waters), mangrove forests, bushes and other coastal land-vegetation, also rice fields and housings. This map, in a geographic information system (GIS) format, can be used for fieldwork, as base maps for other scientific studies and for management of coral reef ecosystem.

3.3 Spectroradiometric measurements

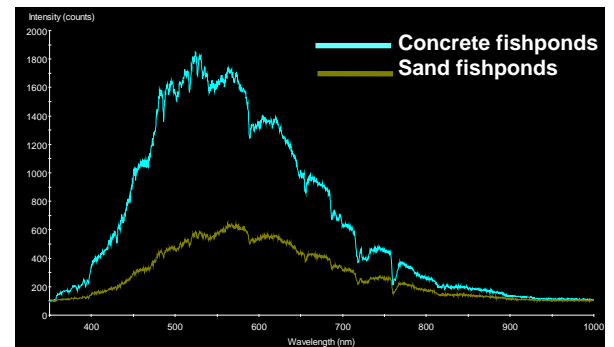
In-situ spectroradiometric measurements play an important role in the development of remote sensing applications, bridging the gap between laboratory optical measurements and measurements from satellite platforms (Dekker et al. 1992). Therefore, this study also measure reflectance properties of various objects. Averaged reflectance spectra for the coastal vegetation, including two species of mangroves, different types of coastal substrates, fishponds, and different types of seawater are shown in Figure 7.



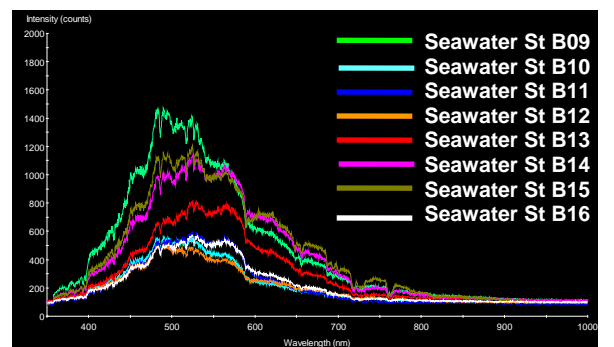
(a)



(b)



(c)



(d)

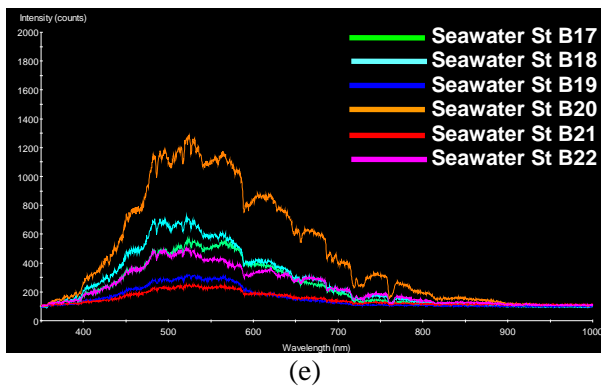


Figure 7. Observed spectral reflectance of coastal vegetation (a), coastal substrate (b), fishponds (c), and different types of seawater (d, e).

There were two types of fishponds for reflectance measurement, i.e. concrete-based and sand-based. The concrete fishponds spectra had the highest reflectance values (Figure 7c). The coastal vegetation had lower reflectance compared to different coastal land-substrate (Figure 7a and 7b). This indicated that bare sediment around the coasts could be easily separated from other bottom types on the basis of brightness alone.

All coastal vegetation showed a reflectance maximum at around 750 nm, and mangrove reflectance spectra showed the most variation in shape and magnitude within species in comparison with the other groups (Figure 7a). Within them *Rhizophora* had the lowest reflectance values and the least variation in spectral shape (Figure 7a). Figure 7d and 7e illustrate that turbid seawaters have higher reflectance in comparison to clear seawaters. All turbid seawaters exhibit a reflectance maximum at around 500 nm.

4. CONCLUSION

FORMOSAT-2 is able to provide high-quality satellite images for coastal environment mapping. Results from spectroradiometric measurements indicate that:

- (1) for the purpose of medium (community) and fine (species) vegetation mapping, it is best to use spectral band B2 and B4 of FORMOSAT-2.
- (2) for the purpose of coastal seawater and sediment mapping, it is best to use spectral band B1 and B2 of FORMOSAT-2
- (3) for the purpose of fish ponds mapping, it is best to use spectral band B2 and B3 of FORMOSAT-2

ACKNOWLEDGMENTS

This research was supported by the Agency for Marine and Fishery Research of the Indonesian Ministry of Marine Affairs and Fisheries, Department of Marine Science and Technology of Bogor Agricultural University, Agency for the Assessment and Application of Technology, and counterparts in Chinese Taipei especially in providing valuable FORMOSAT-2 data. The assistance of several colleagues during fieldwork is gratefully acknowledged. Special thanks to Adriani whose comments were greatly appreciated in contributing to the final form of this paper.

REFERENCES

- Dekker AG, Malthus TJ, Wijnen MM, Seyhan E (1992) The effect of spectral bandwidth and positioning on the spectral signature analysis of inland waters. *Remote Sens. Environ.* 41: 211–225
- DEPKIMPRASWIL. 2003. *Buku Profil Penataan Ruang Provinsi Banten*. Direktorat Jenderal Penataan Ruang. Departemen Pemukiman dan Prasarana Wilayah.
- English, C. Wilkinson and V. Baker (Eds.). 1997. *Survey Manual for Tropical Marine Resources* 2nd Edition. Australian Institute of Marine Science.
- Green EP, Mumby PJ, Edwards AJ, Clark CD (2000) *Remote sensing handbook for tropical coastal management*. UNESCO, Paris
- Tomascik, T, AJ Mah, A Nontji, and MK Moosa. 1997. *The ecology of the Indonesian seas, part 2*. Periplus editions.

Integration of Satellite Application and Computational Tool for Marine Conservation Area Planning

*E. Elvan Ampou, Frida Sidik and Candhika Yusuf
Institute for Marine Research and Observation
Bali, Indonesia*

ABSTRACT

The design of a marine conservation area or so called Kawasan Konservasi Laut (KKL) should meet the goals of KKL itself. The objectives for each type of marine conservation area are varies and almost exclusively focused on habitat protection which leads to the conservation of biological diversities and sustainable fisheries. Satellite application has been widely used to support marine designs. This paper describes how we incorporate data on the spatial distribution of key coastal habitats (such as mangrove and coral reef) and water quality with coastal hydrodynamic model for the design of marine conservation area. The study employs field observation, satellite data processing and modeling. Using a computational tool called MARXAN, we combine those biological and physical information as the primary drivers for the selection of sites for marine reserves. The site location is in Pemuteran, Buleleng, Bali.

Keywords: Kawasan Konservasi Laut (KKL), Biological diversity, MARXAN.

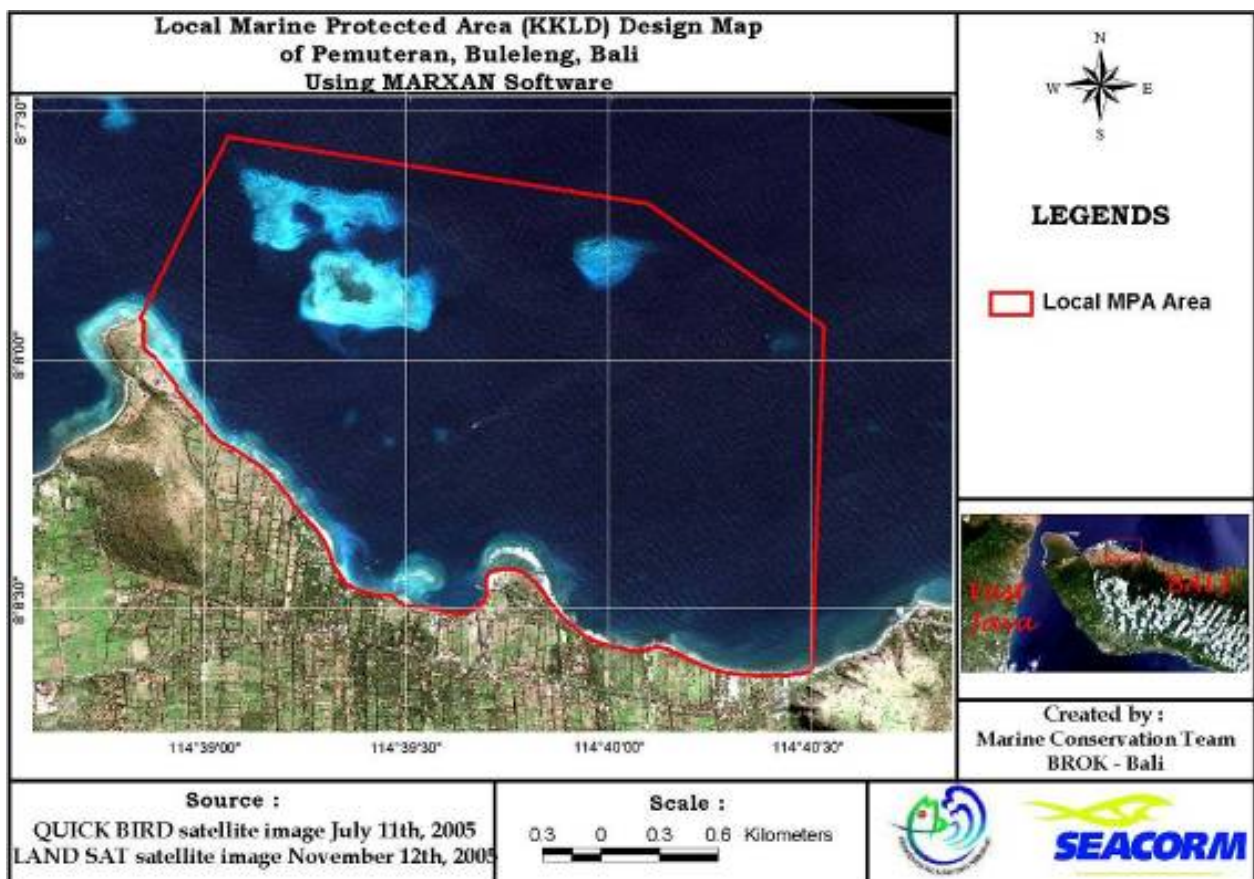


Figure 1. Design Map of MPA in Pemuteran (North Bali) using MARXAN

Biodiversity is defined, and the importance of and threats to marine biological diversity are assessed. A review of current scientific knowledge with respect to marine biological diversities are presented, along with commentary on the particular threats to diversity in the various types of marine ecosystem. This is followed by a general discussion of the ways in which government and the public can protect marine biological diversity to support Marine Conservation Area Planning with integrated to satellite application and computational tool.

1. METHODS

1.1 Time and Place

The Surveys of Coral Reef were carried out in September 9th 2007 until September 10th 2007 at the Pemuteran, Buleleng. (North of Bali).

1.2 Equipments

Table 1. Equipments

Equipments	Function
Jukung boat and speed boat	Transportation
Rope 18 meters	To draw manta tow surveyor
Manta board	Data board
Pencil	Write data
Masker, Snorkel, Fins	Skin Dive
SCUBA Gear	Diving
String Liners (50 meters)	Line Transect
GPS (Global Positioning System)	To acquires point of coordinate
Stopwatch / jam	To acquires point of time
Underwater camera	Documentation

1.3 . Manta Tow

The purposes of Manta Tow method are for assessing broad-scale changes in reef cover due to cyclone damage, coral bleaching and outbreaks of the Crown-of-thorns starfish, *Acanthaster planci*. A good synopsis of the method is given in [English et al.](#) (1997) which forms the basis of the following description.

The category or percent cover refers to Rogers, C., Garrison, G., Grober, R., Hillis, Z-M., dan Franke, M.A. (1994) figure 2.

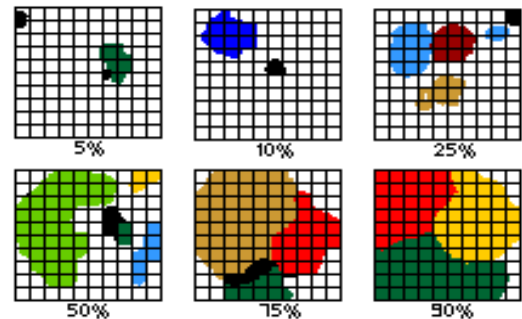


Figure 2. Percentage of Life Form

1.4 Coral Reef Survey

The Line Intercept Transects (LIT) is fairly rapid to deploy in field. A fiber glass tape measure is laid close to the reef contour and the length (cover) of each reef category is recorded. A faster variant is the point intercept transect in which only the type of reef category is noted at equidistant points along the line (e.g. every 20 cm). The cover of each category is calculated by the ratio of number of points per category to the total number of points. The main limitation with line and point intercept transects is that they tend to under-sample heterogeneous areas with low cover of reef categories (e.g. areas of scattered corals) (English et al., 1997). Transect throughout 50 meters in depth 5 and 10 meters cross the coast line.

The function of this method is to describe the percent cover of life form.

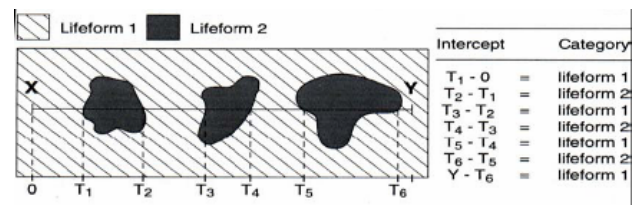


Figure 3. Line Intercept Transect method (English et al, 1997).

Table 2. Remarks of *benthic life form*

<i>benthic life form code</i>	Description
ACB	Acropora branching
AEN	Acropora encrusting
ASM	Acropora sub massive
CA	Coraline Algae
CE	Coral Encrusting
CF	Coral Foliosa
CM	Coral Massive
CSM	Coral Sub Massive
DC	Dead Coral
DCA	Dead Coral Alge
<i>Diploastrea heliopora</i>	<i>Diploastrea heliopora</i>
EUP	Euphyllia
FAV	Faviidae
FNG	Fungia
GAL	Galaxea
GON	Goniopora
Millepora	Millepora
MNT	Montipora
PAC	Pachyseris
PBR	Porites Branching
PEC	Pectinia
PLA	Platygyra
POC	Pocilopora
POR	Porites
RB	Rubble
RCK	Rock
SC	Soft Coral
SD	Sand
SER	Seriatopora
SPG	Sponge
T.squamosa	<i>Tridacna squamosa</i>
Tunicate	Tunicate

(English *et al.*, 1997)

1.5 Reef Fish Survey

The basic principle of plot-less Belt Transects is similar to the manta tow, the main difference being that observers are not towed behind a boat. This affords a useful means of independence allowing the use of scuba and permitting very shallow areas to be surveyed safely. Since the observer can get much closer to the sea bed, it is possible to record more detailed data on bottom features. In the species-rich Indo-Pacific, this may include coral and algal life forms include Reef Fish (for examples, see English *et al.* 1997)

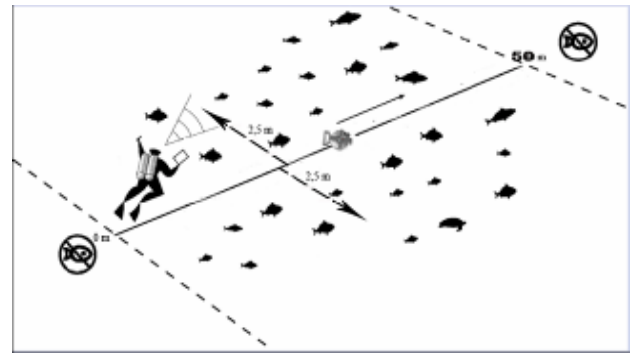
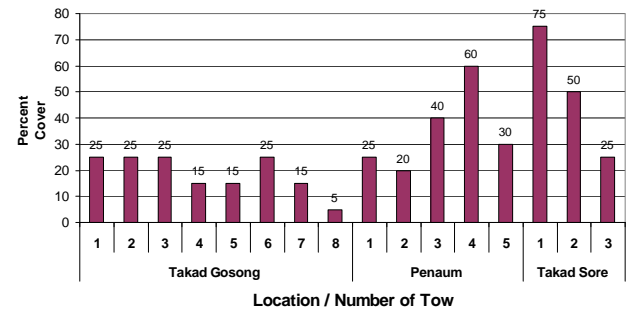


Figure 4. Visual Census use Belt Transect Method (English *et al.*, 1997)

2 RESULT AND DISCUSSION

2.1 Manta Tow



Graphic 1. Percent Cover of Life Form

Based from the manta tow surveys on *Pemuteran* area, “Takad Sore” and “Penaum” were included in the category of “Damaged to Recovery” Life Form. Whereas in “Takad Gosong” the percent cover of life form were included in the category of “Damaged to Critical” Life Form.

3. CORAL REEF

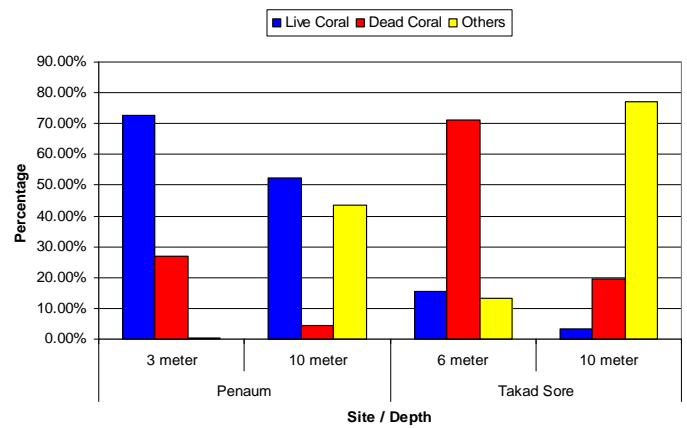
3.1. Percent Cover

Based from the LIT surveys on coral reef, indicates that in “Penaum” have a higher percentage of life form than “Takad Sore”. Penaum = 72.74 % in the deepness 3 m and 52.20 % in the deepness 10 meters (Healthy Lifeform). Mean while in Takad Sore = 15.48 %; 6 m and 3.40 %; 10 m which included in the category of damaged/critically.

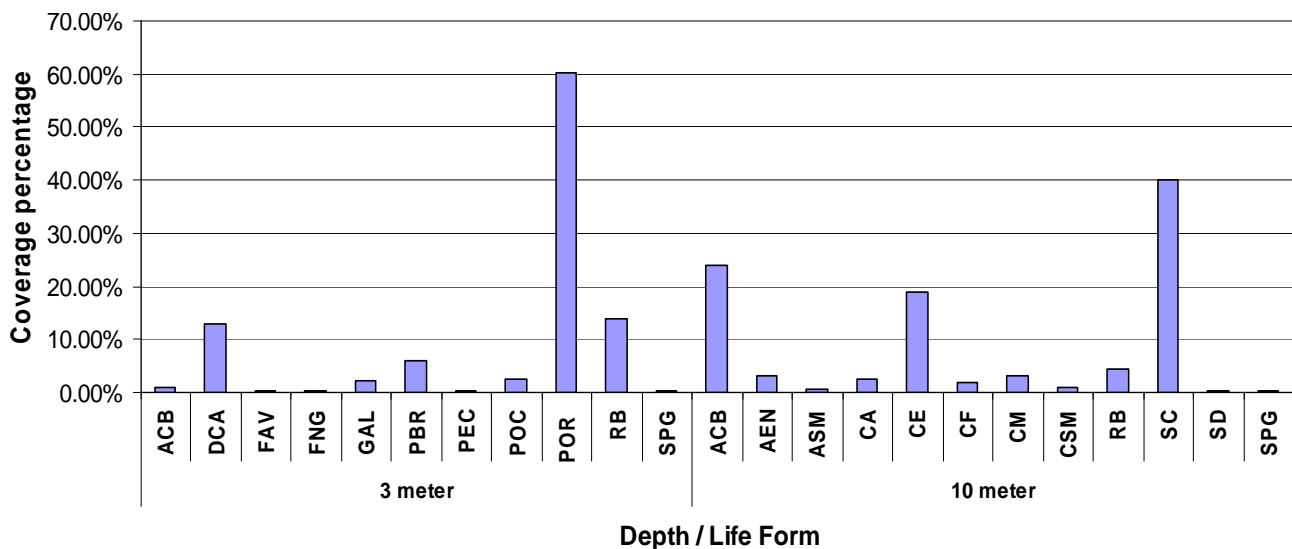
Table 3. Benthic Life Form distribution in two side (Penaum and Takad Sore)

No	Life Form	Penaum	Takad Sore
1	ACB	+	+
2	AEN	+	-
3	ASM	+	-
4	CA	+	+
5	CE	+	-
6	CF	+	-
7	CM	+	+
8	CSM	+	+
9	DC	-	+
10	DCA	+	+
11	<i>Diploastrea heliopora</i>	-	+
12	EUP	-	+
13	FAV	+	+
14	FNG	+	+
15	GAL	+	+
16	GON	-	+
17	MILLEPORA	-	+
18	MNT	-	+
19	PAC	-	+
20	PBR	+	-
21	PEC	+	+
22	PLA	-	+
23	POC	+	+
24	POR	+	+

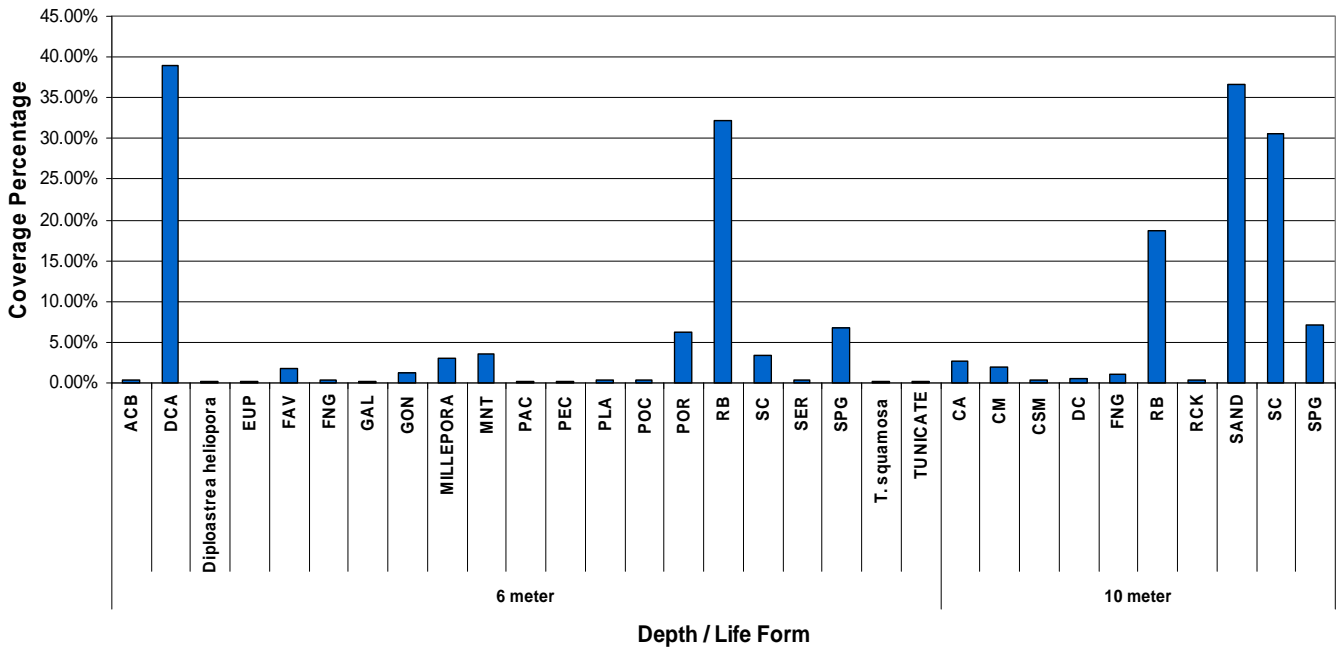
25	RB	+	+
26	RCK	-	+
27	SC	+	+
28	SD	+	+
29	SER	-	+
30	SPG	+	+
31	T. squamosa	-	+
32	TUNICATE	-	+



Graphic 2. The Ratio of Death Coral, Life Coral and *others* in two sites

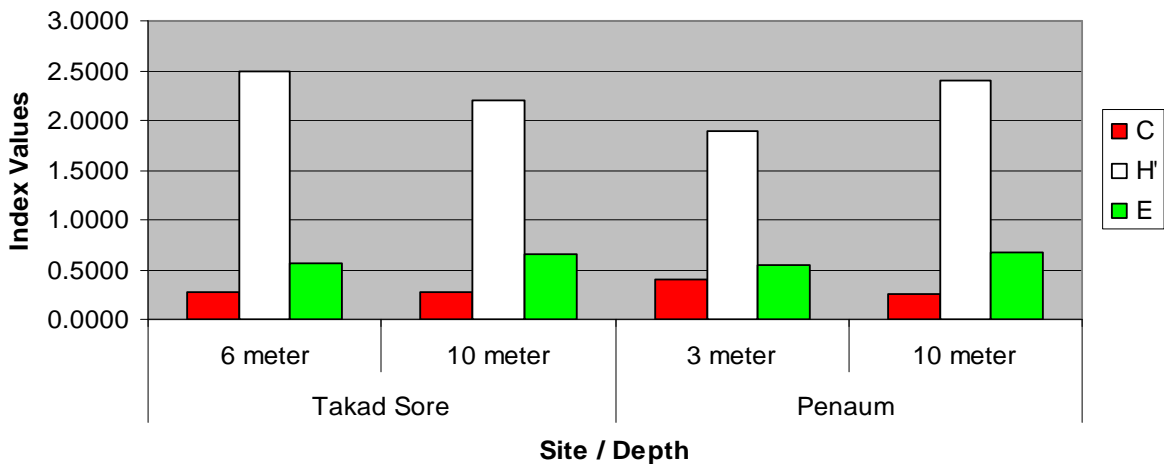


Graphic 3. Percent Cover of Benthic Life Form in Penaum



Graphic 4. Percent Cover of Benthic Life Form in Takad Sore

3.2 Coral Reef's Ecology Index



Graphic 5. Index Ecology ratio of Coral Reef at two sites

Based on the ecological index values, “Takad Sore” have a low domination level (C = 0.2674; 6m and 0.2686; 10m) with a small diversity level (H = 2.4917; 6 m and 2.2024; 10 m) and the uniformity level medium to high (E = 0.5673; 6 m and 0.6671; 10 m).

Such as well in “Penaum” have a low domination level (C = 0.4039; 3 m and 0.2579; 10 m) with a small diversity level (H = 1.8825; 3 m and 2.3915;10 m) and the uniformity level medium to high (E = 0.5442; 3 m and 0.6671; 10 meter).

4. REEF FISH

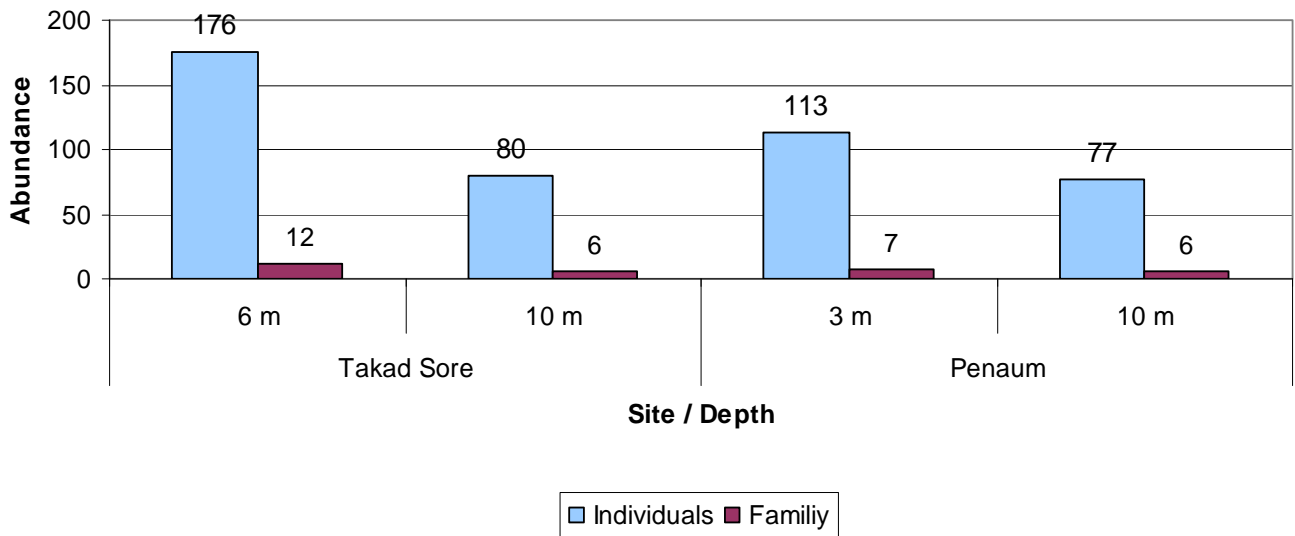
4.1. Reef Fish Abundant r

Based from *visual census* on the belt transect method, there were a total of 446 individuals from 15 families of reef fish. In “Takad Sore” = 256 individuals from 15 families of reef fish.

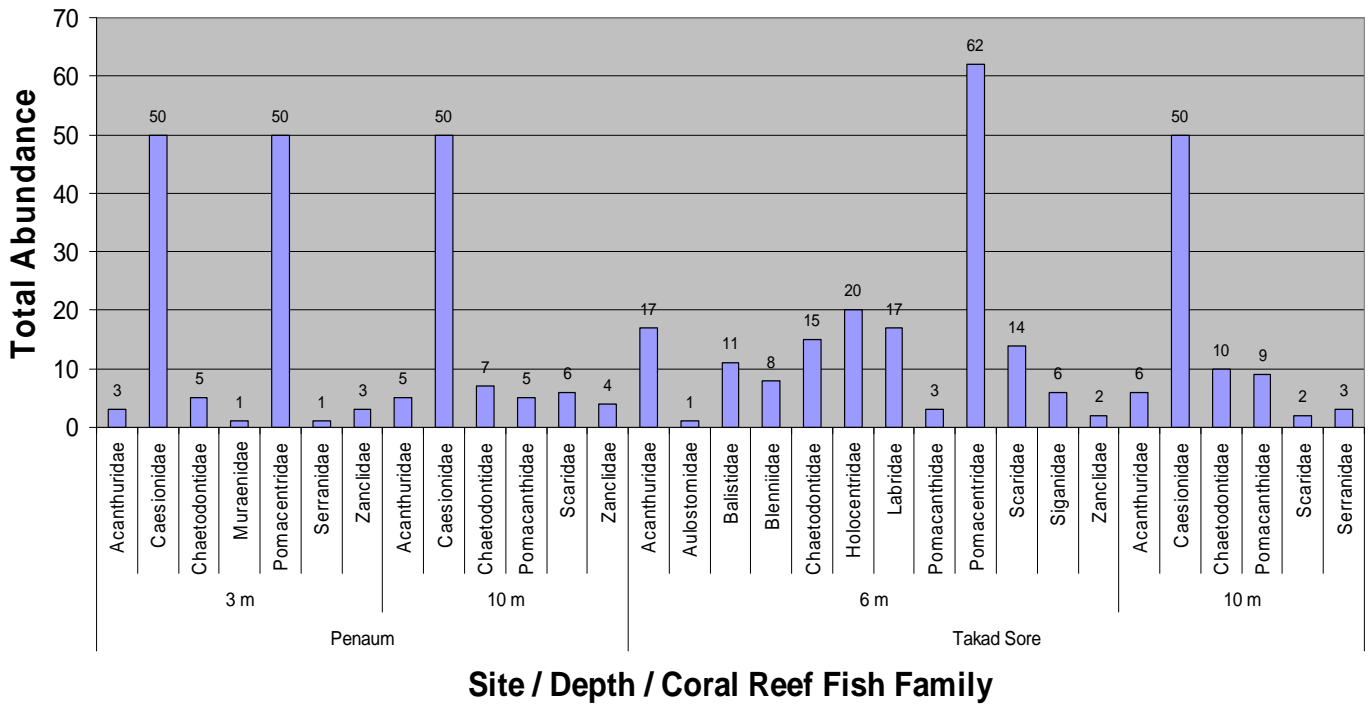
The reef fish families encountered during the surveys such as *Acanthuridae* (*Surgeonfishes*) and *Chaetodontidae* (*Butterflyfishes*), where as the most encountered reef fish families were *Caesionidae* (*Fusiliers*) and *Pomacentridae* (*Damselfishes*).

Table 4. Reef Fish Family Presence.

No.	Reef Fish Family	Family Presence			
		Takad Sore		Penaum	
		6 m	10 m	3 m	10 m
1	Acanthuridae	+	+	+	+
2	Aulostomidae	+	-	-	-
3	Balistidae	+	-	-	-
4	Bleenniidae	+	-	-	-
5	Caesionidae	-	+	+	+
6	Chaetodontidae	+	+	+	+
7	Holocentridae	+	-	-	-
8	Labridae	+	-	-	-
9	Muraenidae	-	-	+	-
10	Pomacanthidae	+	+	-	+
11	Pomacentridae	+	-	+	-
12	Scaridae	+	+	-	+
13	Serranidae	-	+	+	-
14	Siganidae	+	-	-	-
15	Zanclidae	+	-	+	+

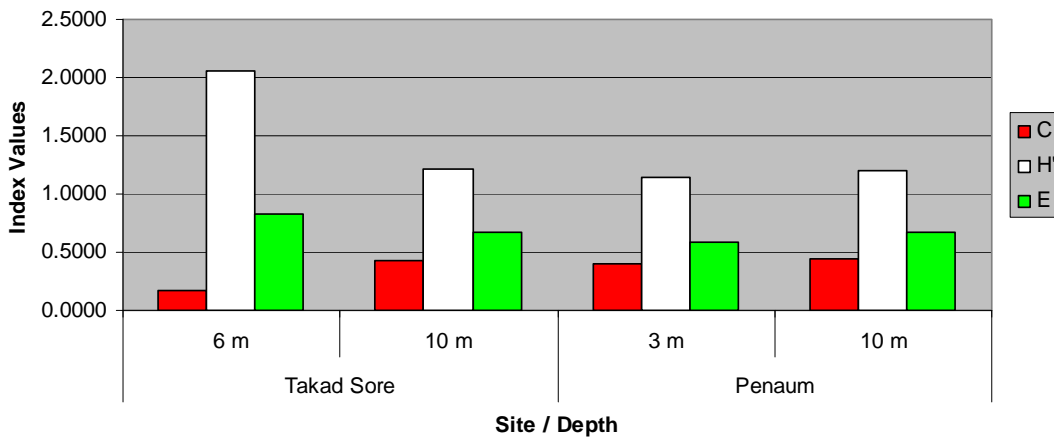


Graphic 6. Reef Fish Abundant



Graphic 7. Reef Fish Abundant and Total Individual per Family

4.2. Coral Reef Fish's Ecology Index



Graphic 7. Index Ecology ratio of Coral Reef Fish at two sites

Based on the ecological indexes calculation result, "Takad Sore" have low domination index values (C = 0.1768 at the depth of 6 meter and C = 0.4266 at 10 meter depth), average values of diversity index (H = 2.0561 at the depth of 6 meter and H = 1.2091 at 10 meter depth) and average to

high evenness index values (E = 0.8274 at the depth of 6 meter and E = 0.6748 at 10 meter depth).

The similar results were also occurred at "Penaum" where it have low domination index values (C = 0.3951 at the depth of 3 meter and C = 0.4471 at 10 meter depth), average values of

diversity index ($H = 1.1359$ at the depth of 3 meter and $H = 1.2060$ at 10 meter depth) and average to

high evenness index values ($E = 0.5837$ at the depth of 3 meter and $E = 0.6731$ at 10 meter depth).

5. APPLIED TO MARXAN

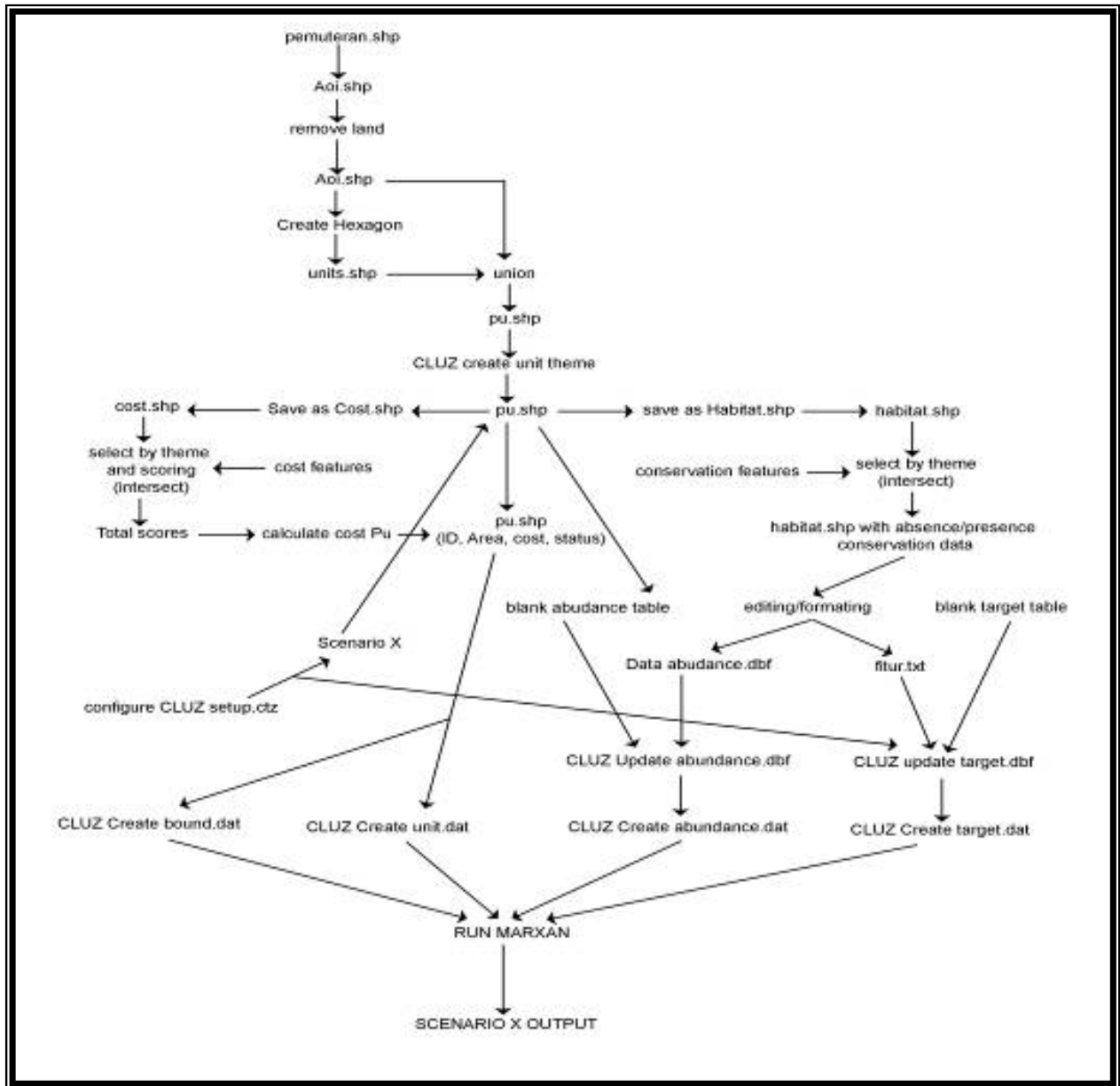
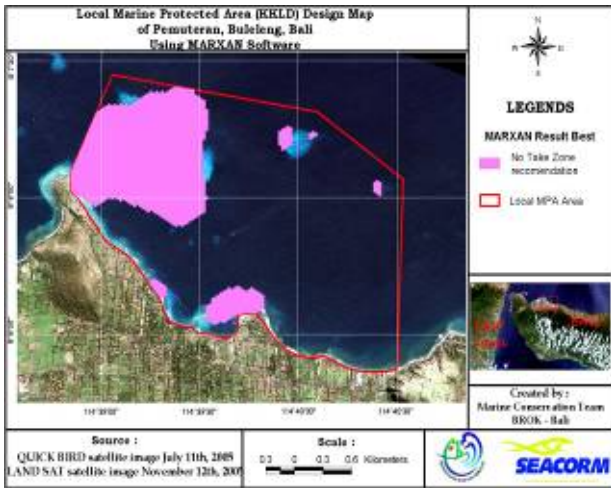


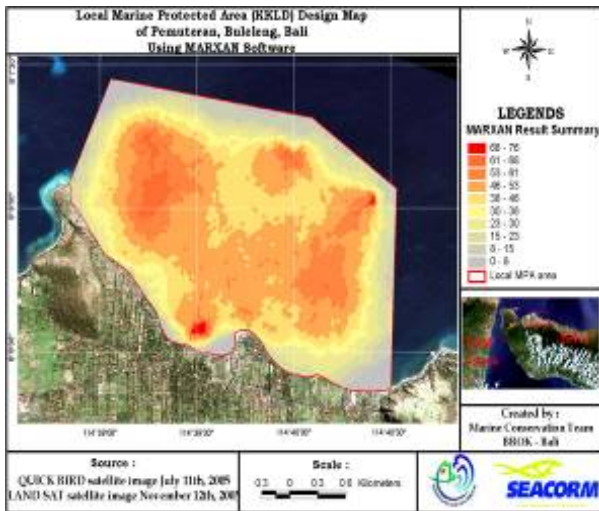
Figure 5. Flowchart of Running Marxan

6. SURVEY DOCUMENTATIONS

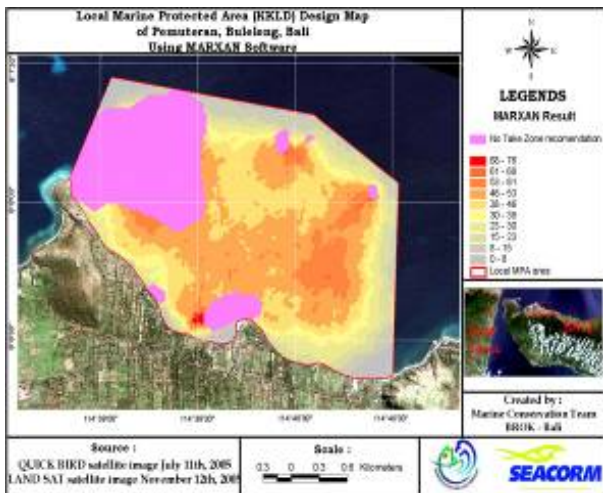
(Photo by : Elvan Ampou and Candhika Yusuf)



Manta Tow survey



Diversities of soft coral founded at Takad Sore



Coral of Genus Platygyra at Takad Sore

Figure 6. Local Marine Protected Area Using Marxan Software at Pemuteran – Buleleng, Bali.



Line Intercept Transect (LIT) survey



Diversities of coral reef fishes at Takad Sore



Tridacna squamosa at Takad Sore

REFERENCES

- Allen, G. Steene, R. Humann, P dan Deloach, N. 2003. Reef Fish Identification : Tropical Pacific. Star Standard Industries. Pte Ltd. Singapore. 457 pp.
- Azhar, I. dan E.N. Edinger. 1996. Ekotipologi Terumbu Karang pada Perairan P. Cemara Kecil, P. Menyawakan dan Gosong Cemara, Taman Nasional Laut Karimunjawa. Sub BKSDA Jawa Tengah dan Universitas Diponegoro – McMaster University Project. Semarang
- English S, C.Wilkinson, V. Baker (eds).1997. Survey Manual for Tropical Marine Resources (2nd Edition). Australian Institute of Marine Science. ASEAN-Australia Marine Project
- Krebs, C.J. 1985. The Experimental Analysis of Distribution and Abundance Third edition. Harper and Row Publishers. New York.
- Legendre, L. dan P. Legendre. 1983. Numerical Ecology. Elsevier Science Publication. New York
- Ludwig JA, Reynolds JF, 1988, Statistical ecology: a primer on methods and computing. Wiley-Interscience Publications. New York
- Odum, E. P. 1971. Fundamental of Ecology. Third Edition. W. B. Sanders Company. Toronto. 574 pp.
- Pielou C. 1966. The measurement of diversity on different types of biological collections. Amer. Nat. 94:25-36.
- Rogers, C., Garrison, G., Grober, R., Hillis, Z-M., and Franke, M.A., 1994, Coral Reef Monitoring Manual for the Caribbean and Western Atlantic. (St. John: National Park Service, Virgin Islands National Park).
- Sukarno. 1994. Ekosistem Terumbu Karang dan Masalah Pengelolaannya. Materi Kursus Pelatihan Metodologi Penelitian Penentuan Kondisi Terumbu Karang. P3O LIPI. Jakarta
- Sukmara A., A.J. Siahainenia., C. Rotinsulu, C. 2001. Panduan Pemantauan Terumbu Karang Berbasis – Masyarakat Dengan Metoda Manta Tow. Proyek Pesisir. Publikasi Khusus. University of Rhode Island, Coastal Resources Center, Narragansett, Rhode Island, USA.